

The 2dF Galaxy Redshift Survey: The b_J-band galaxy luminosity function and survey selection function

Peder Norberg¹, Shaun Cole¹, Carlton M. Baugh¹, Carlos S. Frenk¹, Joss Bland-Hawthorn², Terry Bridges², Russell Cannon², Matthew Colless³, Chris Collins⁴, Warrick Couch⁵, Nicholas J.G. Cross⁶, Gavin Dalton⁷, Roberto De Propris⁵, Simon P. Driver⁶, George Efstathiou⁸, Richard S. Ellis⁹, Karl Glazebrook¹⁰, Carole Jackson³, Ofer Lahav⁸, Ian Lewis⁷, Stuart Lumsden¹¹, Steve Maddox¹², Darren Madgwick⁸, John A. Peacock¹³, Bruce A. Peterson³, Will Sutherland¹³, Keith Taylor² (The 2dFGRS Team)

¹Department of Physics, University of Durham, Science Laboratories, South Road, Durham DH1 3LE, United Kingdom

²Anglo-Australian Observatory, P.O. Box 296, Epping, NSW 2121, Australia

³Research School of Astronomy & Astrophysics, The Australian National University, Weston Creek, ACT 2611, Australia

⁴Astrophysics Research Institute, Liverpool John Moores University, Twelve Quays House, Egerton Wharf, Birkenhead, L14 1LD, UK

⁵Department of Astrophysics, University of New South Wales, Sydney, NSW2052, Australia

⁶School of Physics and Astronomy, North Haugh, St Andrews, Fife, KY16 9SS, United Kingdom

⁷Department of Physics, Keble Road, Oxford OX1 3RH, United Kingdom

⁸Institute of Astronomy, University of Cambridge, Madingley Road, Cambridge CB3 0HA, United Kingdom

⁹Department of Astronomy, California Institute of Technology, Pasadena, CA 91125, USA

¹⁰Department of Physics & Astronomy, Johns Hopkins University, 3400 North Charles Street Baltimore, MD 212182686, USA

¹¹Department of Physics & Astronomy, E C Stoner Building, Leeds LS2 9JT, United Kingdom

¹²School of Physics and Astronomy, University of Nottingham, University Park, Nottingham, NG7 2RD, United Kingdom

¹³Institute of Astronomy, University of Edinburgh, Royal Observatory, Edinburgh EH9 3HJ, United Kingdom

2 December 2024

ABSTRACT

We use more than 110 500 galaxies from the 2dF galaxy redshift survey (2dFGRS) to estimate the b_J-band galaxy luminosity function at redshift $z = 0$, taking account of evolution, the distribution of magnitude measurement errors and small corrections for incompleteness in the galaxy catalogue. Throughout the interval $-14 > M - 5\log_{10} h > -22$, the luminosity function is accurately described by a Schechter function with $M_{b_J}^* - 5\log_{10} h = -19.66 \pm 0.07$, $\alpha = -1.21 \pm 0.03$ and $\Phi^* = (1.68 \pm 0.08) \times 10^{-2} h^3 \text{Mpc}^{-3}$, giving an integrated luminosity density of $\rho_L = (1.9 \pm 0.18) \times 10^8 h L_\odot \text{Mpc}^{-3}$ (assuming an $\Omega_0 = 0.3$, $\Lambda_0 = 0.7$ cosmology). The quoted errors have contributions from the accuracy of the photometric zeropoint, large scale structure in the galaxy distribution and, importantly, from the uncertainty in the appropriate evolutionary corrections. Our luminosity function is in excellent agreement with, but has much smaller statistical errors than an estimate from the Sloan Digital Sky Survey (SDSS) data when the SDSS data are accurately translated to the b_J-band and the luminosity functions are normalized in the same way. We use the luminosity function, along with maps describing the redshift completeness of the current 2dFGRS catalogue, and its weak dependence on apparent magnitude, to define a complete description of the 2dFGRS selection function.

Key words: galaxies: luminosity function - selection function - 2dF galaxy redshift survey (2dFGRS) - mock catalogues

1 INTRODUCTION

The galaxy luminosity function (LF), which gives the abundance of galaxies as a function of their luminosity, is one

of the most fundamental properties of the galaxy distribution. The accuracy with which it is known has improved steadily as the size of the redshift surveys used to determine it has grown (e.g. Efstathiou, Ellis & Peterson 1988; Loveday et al. 1992; Marzke, Huchra & Geller 1994; Zucca et al. 1997; Folkes et al. 1999; Blanton et al. 2001; Madgwick et al. 2001). Here we present an estimate of the b_J -band luminosity function from the 2dF Galaxy Redshift Survey (2dFGRS) which is currently the largest galaxy redshift survey in existence. The luminosity function is an important statistic in its own right and understanding how it arises is a major goal of models of galaxy formation (e.g. White & Frenk 1991; Kauffmann, White & Guiderdoni 1993; Cole et al. 1994, 2000; Somerville & Primack 1999). Also to exploit the 2dFGRS fully, it is important to have an accurate model of the luminosity function so that the selection function of the survey can be determined. This is a vital ingredient in analysing all aspects of galaxy clustering within the survey.

This paper presents an estimate of the overall b_J -band galaxy luminosity function. This estimate takes account of k -corrections (which result from the redshifting of the measured wavelength range) and also average evolutionary corrections. We also include the effects of photometric errors and small corrections for incompleteness in the survey, however we do not include surface brightness corrections which will be discussed in Cross et al. (2001b). The analysis presented here is complementary to that in Madgwick et al. (2001) and the earlier analysis in Folkes et al. (1999). In these cases a subset of the 2dFGRS data were analyzed with the primary aim of establishing how the luminosity function depends on spectral type. These papers did not apply evolutionary corrections since they were not attempting to model the full selection function of the survey. We compare and discuss our result in relation to these and other recent determinations of the luminosity function, including that from the Sloan Digital Sky Survey (SDSS). We also compare estimates for different regions of the survey to test the uniformity of the catalogue and our model assumptions. Throughout, we use mock galaxy catalogues constructed from the Hubble Volume N-body simulations (Evrard 1999; Evrard et al. 2001) in order to check our methods and to assess the influence of large scale structure upon our results. We also use the estimated luminosity function and our modelling of the survey selection limits and completeness to produce a complete description (angular, redshift and apparent magnitude) of the 2dFGRS selection function. The predictions of this selection function are compared with various properties of the real catalogue including the galaxy number counts and redshift distributions.

The paper is divided into 10 sections. In Section 2 we describe all the relevant details of the 2dFGRS. We discuss the accuracy of the photometry and review the accuracy of the redshifts and various aspects of the completeness of the photometric and redshift catalogues. In Section 3 we describe how we model the galaxy $k+e$ corrections. In Section 4 we briefly describe a set of mock catalogues, which we use to both test our implementation of the luminosity function estimators and to assess the effects of large-scale structure. We present a series of luminosity function estimates in Section 5, where we compare results for different regions and subsets of the survey. In Section 6 we examine the 2dFGRS number counts that we use to normalize our LF estimates

and compare them to counts from the SDSS. Our normalized estimate of the 2dFGRS luminosity function is presented in Section 7. We compare our results with independent LF estimates in Section 8. In Section 9 we use our best estimate of the 2dFGRS LF, together with the description of the survey magnitude limits and completeness, to construct a model of the survey selection function. From this we extract the expected redshift distribution which we compare with those of the real survey and mock catalogues. We discuss our results and present our conclusions in Section 10.

2 THE 2dF GALAXY REDSHIFT SURVEY

The 2dFGRS is selected in the photographic b_J band from the APM galaxy survey (Maddox et al. 1990a, 1990b, 1996) and subsequent extensions to it, that include a region in the northern galactic cap (Maddox et al. 2001). The survey covers approximately 2151.6 deg^2 in two broad declination strips. The larger of these is centred on the South Galactic Pole (SGP) and approximately covers $-22^\circ.5 > \delta > -37^\circ.5$, $21^\circ 40^\text{m} < \alpha < 3^\circ 40^\text{m}$; the smaller strip is in the northern galactic cap and covers $2^\circ.5 > \delta > -7^\circ.5$, $9^\circ 50^\text{m} < \alpha < 14^\circ 50^\text{m}$. In addition, there are a number of pseudo-randomly located circular 2-degree fields scattered across the full extent of the low extinction regions of the southern APM galaxy survey. There are some gaps in the 2dFGRS sky coverage within these boundaries due to small regions that have been excluded around bright stars and satellite trails. The aim of the 2dFGRS is to measure the redshifts of all the galaxies within these boundaries with extinction-corrected b_J magnitudes brighter than 19.45. As described in Colless et al. (2001), this is achieved by dividing the target galaxies among a series of overlapping 2° diameter fields. The degree of overlap of the fields is such that the number of targets assigned to each field is no greater than the 400 fibres that the 2dF instrument uses to obtain spectra for each target simultaneously. When all these 2° fields have been observed, in early 2002, close to 250 000 galaxy redshifts will have been measured.

In this paper we use the 153 986 redshifts obtained prior to May 2001 in the main NGP and SGP strips. This sample covers a large fraction of the full 2dFGRS area, but as shown in Fig. 1, within this area the sampling rate varies with position on the sky. This is a direct consequence of some of the overlapping 2° fields having not yet been observed and so is well understood and can be accurately modelled (see section 8 of Colless et al. 2001).

For accurate statistical analysis of the 2dFGRS it is essential to understand fully the criteria that define its parent photometric galaxy catalogue and also the spatial and magnitude dependent completeness of the redshift catalogue. Here we complement the description given in the survey construction papers (Maddox et al. 2001; Colless et al. 2001) by making a direct comparison of the 2dFGRS catalogue in the overlap with the Early Data Release (EDR) of the Sloan Digital Sky Survey (SDSS). The two datasets have approximately 30 000 galaxies in common of which about 10 000 have redshift measurements in both surveys. In the following section we use these data to assess the accuracy of the 2dFGRS photometry, the completeness of the parent galaxy catalogue and the accuracy of the redshifts.

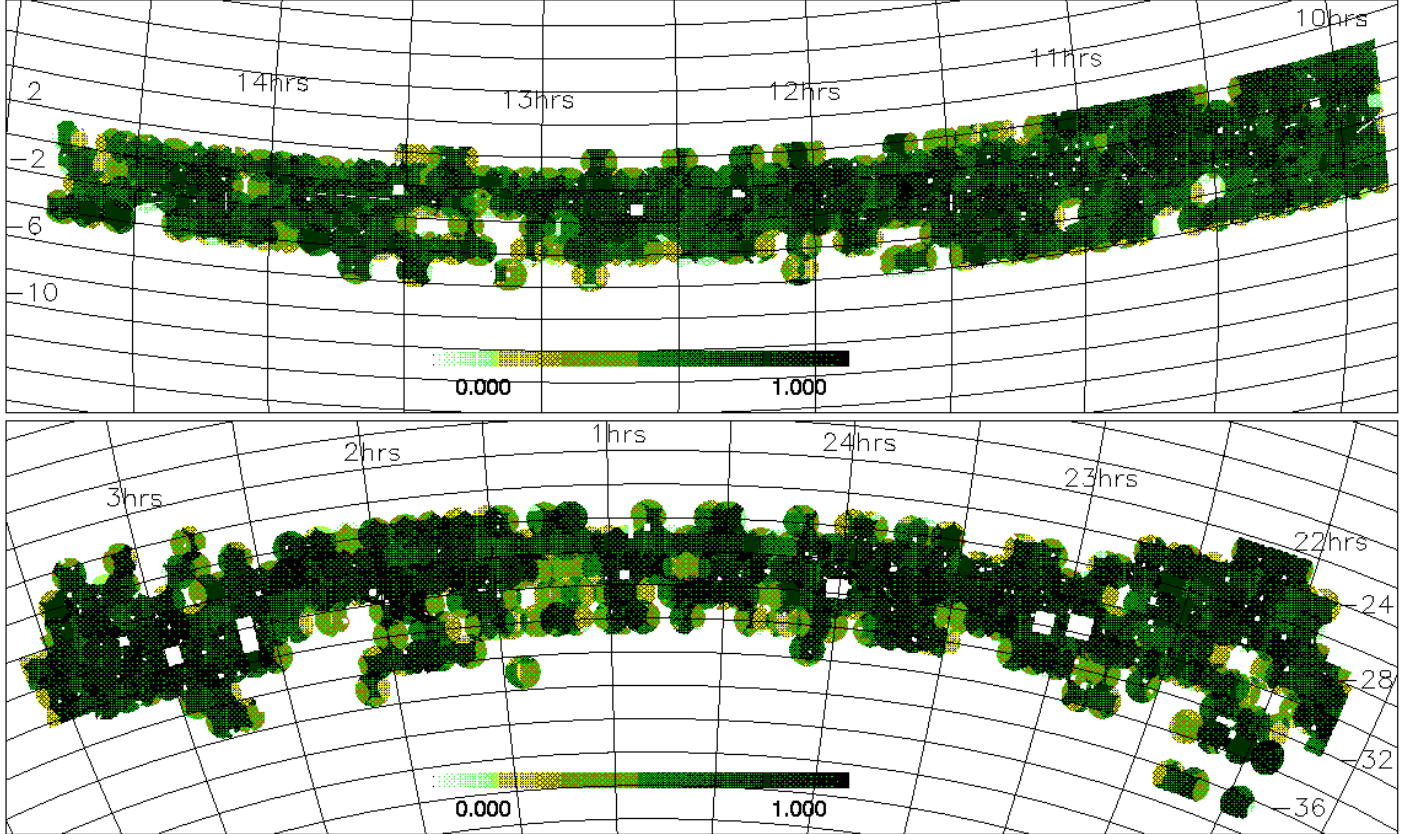


Figure 1. The sky coverage of the 2dFGRS dataset analysed in this paper. This dataset includes galaxy redshifts from all fields observed before May 2001 that have a redshift completeness greater than 70%. As the fields overlap and many are still to be observed, the completeness varies across the sky. The quantity represented by the grey-scale is the sector redshift completeness, $R(\theta)$, defined in Appendix A.

2.1 Photometric Accuracy

The 2dFGRS magnitudes that we use here are the same as those made public in our June 2001 “100k Release”. They are pseudo-total magnitudes measured from APM scans of photographic plates from the UK Schmidt Telescope (UKST) Southern Sky Survey and their precision depends on the accuracy of the zeropoint, and non-linearity corrections of each plate, as well as the measurement errors within each plate. The plate zeropoints and non-linearity corrections are set using a combination of plate overlaps and external CCD photometry. We estimate that the rms plate zeropoint error, for galaxies with magnitudes in the range $17 < b_J < 19.5$, is 0.07 magnitudes. As described in Colless et al. (2001), the individual galaxy magnitudes have a larger scatter with a 68% spread of approximately ± 0.15 magnitudes.

Fig. 2a and b compare 2dFGRS magnitudes with CCD magnitudes from Patch B of European Imaging Survey (EIS; Prandoni et al. 1999). The EIS includes both B and V-band data and we synthesise b_J using the colour equation $b_J = B - 0.28(B - V)$ (Blair & Gilmore 1982). The coefficient in this colour equation is close to the value -0.27 ± 0.02 , that we find empirically from the EIS data. The EIS Patch B data, which fall on just one UKST plate in the SGP region of the 2dFGRS, form part of the CCD data that were used to calibrate the 2dFGRS photometry. In addition we

used the EIS Chandra Deep field data (Arnouts et al. 2001) and also data from the ESO-Sculptor field (Arnouts et al. 1997), which was taken with the same instrument as the EIS data. Together these data set the zeropoint of the 2dFGRS photometry that was made public in our June 2001 “100k Release”. We assumed that the previous CCD photometry had given the correct relative NGP/SGP calibration, and so used the ESO zeropoint in the NGP, even though there is no direct overlap with the ESO data in the NGP. Fig. 2a confirms that the relation between 2dFGRS and EIS magnitude is linear and has a small zeropoint offset, the median 2dFGRS being fainter than EIS by just $|\Delta| = 0.017$ magnitudes. The histogram in Fig. 2b shows the distribution of magnitude differences after the median offset has been subtracted. The dotted curve which describes the core of the distribution quite well is a gaussian with $\sigma = 0.15$, but one can see that the measured distribution has small non-gaussian tails. The remaining panels of Fig. 2 compare 2dFGRS magnitudes with Petrosian CCD magnitudes from the SDSS EDR (Stoughton et al. 2001). Here we have estimated b_J from the SDSS photometry* using the transformation

* The calibration of the magnitudes in SDSS EDR is preliminary. In many of the SDSS papers a superscript asterisk (e.g. $g^* - r^*$) is used to distinguish these magnitudes from those that the SDSS will ultimately provide.

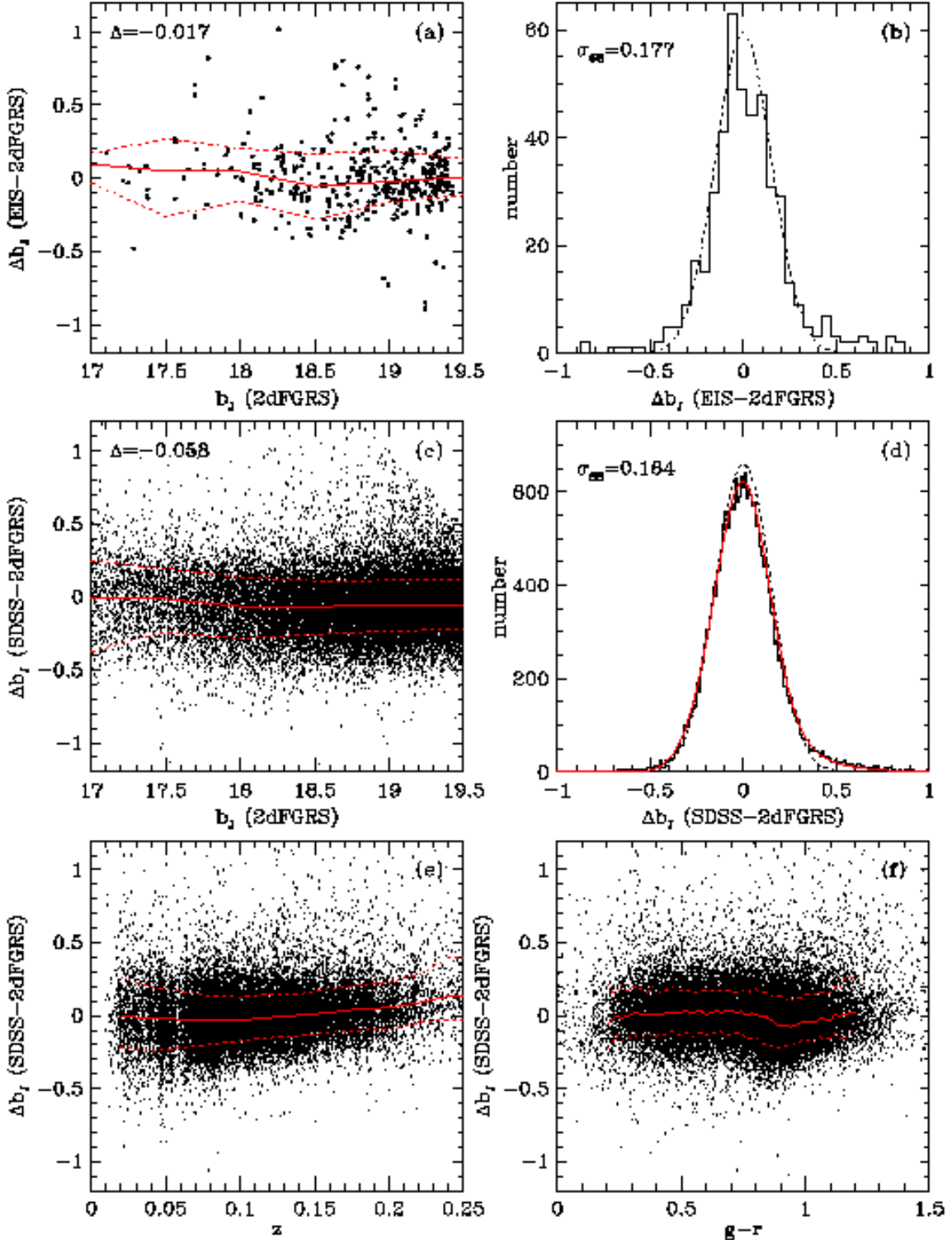


Figure 2. Comparison of 2dFGRS photographic b_J magnitudes and CCD magnitudes from EIS Patch B and SDSS. The upper panels compare the 2dFGRS with the EIS. Panel (a) is a scatter plot of the magnitude difference versus 2dFGRS magnitude and the solid and dotted lines show the magnitude dependence of the median, 16% and 84% quantiles of the distribution. The median magnitude difference, Δ , for all the galaxies in the range $17 < b_J < 19.5$ is indicated on the panel. The distribution of magnitude differences with respect to this median is shown as a histogram in panel (b). The dotted curve, which describes the core of this distribution quite well, is a gaussian with $\sigma = 0.15$ magnitudes. A robust estimate of the width of this distribution, σ_{68} , defined such that $2\sigma_{68}$ spans 68% of the distribution, is also indicated on the panel. Panels (c) and (d) show the corresponding distributions for the comparison of the 2dFGRS and SDSS Petrosian magnitudes. In all but panel (c), the residual is calculated after subtracting the median offset from each UKST plate. The empirical model we adopt to describe the 2dFGRS magnitude measurement errors is shown by the smooth solid curve in panel (d) (see text for details). The lower most panels show the SDSS 2dFGRS magnitude differences versus redshift (e) and $g - r$ colour (f). Again the median, 16% and 84% quantiles are shown.

$$b_J = g + 0.155 + 0.152(g - r). \quad (1)$$

This relation comes from adopting the colour equations given for B and V in Fukugita et al. (1996) and combining these with $b_J = B - 0.28(B - V)$ (Blair & Gilmore 1982), as we did above for the EIS data. Fig. 2f is an empirical test of the colour term in our adopted transformation. The very weak dependence of the median magnitude difference on colour is consistent with the $0.152(g - r)$ colour term and is strongly inconsistent with the colour term $0.088(g - r)$ that was adopted in the comparison between the SDSS and 2dFGRS (Folkes et al. 1999) luminosity function made by Blanton et al. (2001).

Fig. 2c shows that, in the range $17 < b_J < 19.5$, the relation between 2dFGRS and SDSS Petrosian magnitudes is linear and that the scatter between the two measurements is only weakly dependent on magnitude, being slightly greater at brighter magnitudes. There is a zeropoint offset, with the median 2dFGRS magnitude being fainter than that of the SDSS by $|\Delta| = 0.058$ magnitudes. This is not surprising as the zeropoint in the SDSS EDR data is only claimed to be accurate to ± 0.03 magnitudes (Blanton et al. 2001) and similarly the accuracy of the 2dFGRS zeropoint we estimate to be ± 0.04 magnitudes. The SDSS EDR data span 15 UKST plates in the NGP region of the 2dFGRS and there is some plate-to-plate variation in the median offset between 2dFGRS and SDSS Petrosian magnitudes. We find an rms variation of 0.083 magnitudes which is in reasonable agreement with the 0.07 magnitudes rms we estimated from the calibrating photometry, and adds little to the measurement error in an individual galaxy magnitude. We expect the variation in plate zeropoints to be somewhat less in the SGP region of the 2dFGRS as this region was constructed from a more homogeneous set of high quality UKST plates than is available in the NGP. At present there are not enough public CCD data to verify this claim. In the other panels of Fig. 2 the median offset between 2dFGRS and SDSS magnitudes on each plate has been subtracted from the magnitude differences.

The histogram in Fig. 2d shows the distribution of 2dFGRS-SDSS magnitude differences. Again, the dotted curve which describes the core of the distribution quite well is a gaussian with $\sigma = 0.15$. The tail, in excess of this gaussian, of objects for which the 2dFGRS measures a fainter magnitude than the SDSS is very small. There is a somewhat larger tail of objects for which the 2dFGRS measures a brighter magnitude than the SDSS. It is most likely that these objects are close pairs of images which the SDSS has resolved, but which are merged into a single object in the 2dFGRS catalogue. This is precisely what is found for the 2dFGRS when compared to the MGC catalogue (Lemon et al. 2001) by Cross et al. (2001b). Cross et al. (2001b) also find a tendency for the 2dFGRS magnitudes of high surface brightness galaxies to be too faint, as is expected owing to saturation of the UKST plates on scales smaller than the APM spot size (Metcalfe, Fong & Shanks 1995). This correlation makes negligible difference to the overall luminosity function and 2dFGRS selection function. However, it may be an issue for the luminosity function split by spectral type, due to the correlation between spectral type and surface brightness. The overall distribution of magnitude differences is well fitted by the model shown by the solid curve. This

model is the sum of a gaussian and a log-normal distribution. The gaussian component has $\sigma = 0.14$ and accounts for 70% of the probability and the remaining 30% is distributed as a gaussian in $\ln(1 + \Delta b_J)$ with $\sigma = 0.235$. We adopt this model as an empirical description of the distribution of the 2dFGRS magnitude measurement errors. In so doing, we are assuming that the random measurement errors in the SDSS CCD Petrosian magnitudes do not contribute significantly to the width of this distribution. This assumption is consistent with the comparison of the SDSS photometry with the deeper MGC CCD photometry in Cross et al. (2001b).

Fig. 2e shows, for the subset of galaxies for which redshifts have been measured, the magnitude difference as a function of redshift. Below $z \approx 0.16$ there is very little variation in median magnitude difference. At higher redshift there is a weak trend with the 2dFGRS b_J -band magnitude becoming systematically brighter than that inferred from the SDSS. We note that, in contrast, the model of the APM magnitudes constructed by Blanton et al. (2001) falsely predicted that the 2dFGRS magnitude would monotonically become fainter than the SDSS magnitude with increasing redshift. The main reason for the inaccuracy of the Blanton et al. (2001) model is that it neglected to take account of the way in which APM and 2dFGRS magnitudes are calibrated. The calibration of the raw APM magnitudes involves both a zeropoint and a non-linearity correction so that, in principle, for galaxies in each interval of apparent magnitude the median calibrated 2dFGRS magnitude equals the median total magnitude of the calibrating CCD data (Maddox et al. 1990b). The weak variation with redshift seen in Fig. 2e is, in fact, probably due to systematic variation with redshift of the relationship between g , r and b_J magnitudes. The colour equation we have adopted is empirically verified to be accurate for the bulk of the 2dFGRS galaxies, which have a median redshift of $z \approx 0.1$. At higher redshift as different rest frame spectral features pass through the three filter bands one expects small changes in the colour equation.

2.2 Completeness of the 2dF Parent Catalogue

In constructing the parent catalogue of the 2dFGRS the same parameters and thresholds were used to perform star-galaxy separation as in the original APM galaxy survey (Maddox et al. 1990a). Thus, the expectation is that the parent galaxy catalogue will be 90-95% complete and contamination from stellar objects will be 5-10% (Maddox et al. 1990a). In fact, the spectroscopic identification of the 2dFGRS objects shows that the stellar contamination is 5.4% overall and only very weakly dependent on apparent magnitude (see Fig. 3). The SDSS EDR allows us to make a useful test of the 2dFGRS galaxy completeness. In the SDSS commissioning data the star-galaxy classification procedure is expected to be better than 99% complete and have less than 1% stellar contamination (Blanton et al. 2001). In Fig. 3 we assess the completeness of the 2dFGRS parent catalogue both against the SDSS spectroscopic sample and against the SDSS photometric catalogue.

To compare to the SDSS spectroscopic sample we selected all 13 780 SDSS objects that are spectroscopically confirmed as galaxies and have magnitudes brighter than $b_J = 19.5$. The solid histogram in Fig. 3 shows, as a func-

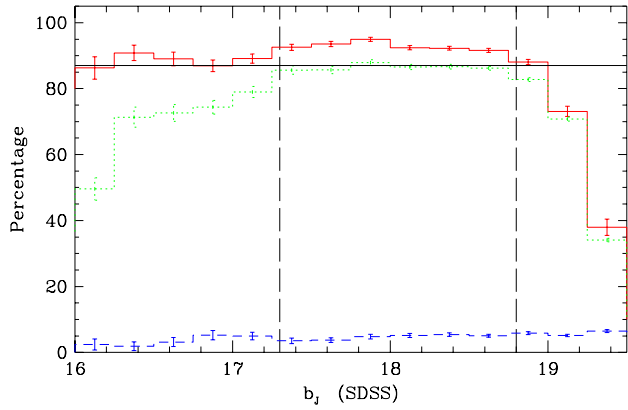


Figure 3. The solid histogram shows, as a function of apparent magnitude, the percentage of spectroscopically confirmed galaxies in the SDSS EDR that have 2dFGRS counterparts. This estimate of the completeness should be ignored rightwards of the vertical dashed line at $b_J = 18.8$. Fainter than this galaxies are absent from the 2dFGRS catalogue simply due to the faint magnitude limit of the catalogue which varies from $19.2 < b_J < 19.5$. The dotted histogram shows the percentage of objects photometrically classified as galaxies, by the $r_{\text{PSF}} - r_{\text{model}} > 0.242$ criterion, in the SDSS EDR. This estimate of the completeness is only reliable between the two vertical dashed lines. The horizontal line indicates our adopted 87% completeness. The dashed histogram shows the percentage of objects in the 2dFGRS parent catalogue in the same area that are spectroscopically identified as stars.

tion of apparent magnitude, the percentage of these galaxies that have counterparts in the 2dFGRS. The completeness varies very little with magnitude over the entire range $16 < b_J < 19.0$. The dip in the estimated completeness evident in the faintest bins is an artifact. Because of random measurement errors in the APM/2dFGRS magnitudes and because the magnitude limit in some parts of the NGP strip is as bright as $b_J \approx 19.2$ (see Colless et al. 2001 figures 13 and 14), some of the selected SDSS galaxies have APM magnitudes that are too faint to be included in the 2dFGRS parent catalogue. Over the magnitude range $17.3 < b_J < 18.8$, indicated by the vertical dashed lines, the completeness is between 91% and 95%.

To compare to the SDSS photometric catalogue we selected all 65 060 SDSS objects that satisfy the star-galaxy classification criteria used by Blanton et al. (2001; i.e. $r_{\text{PSF}} - r_{\text{model}} > 0.242$). This criterion, which compares an estimate of the magnitude of an object assuming it to be a point source with an estimate obtained by fitting a model galaxy template, is very effective at rejecting faint stars from the sample. At magnitudes brighter than $b_J = 17.3$, indicated on Fig. 3 by the leftmost vertical dashed line, the sample becomes contaminated by stars. The dotted histogram in Fig. 3 shows, as a function of apparent magnitude, the percentage of these objects which have counterparts in the 2dFGRS. Brighter than about $b_J = 17.3$, this comparison underestimates the completeness of the 2dFGRS due to the stellar contamination in our SDSS sample. Again in the faintest bins, the 2dFGRS magnitude limit causes the completeness to be underestimated. In the intermediate magnitude range, $17.3 < b_J < 18.8$, between the vertical dashed lines, the completeness is between 85% and 88%. This is sig-

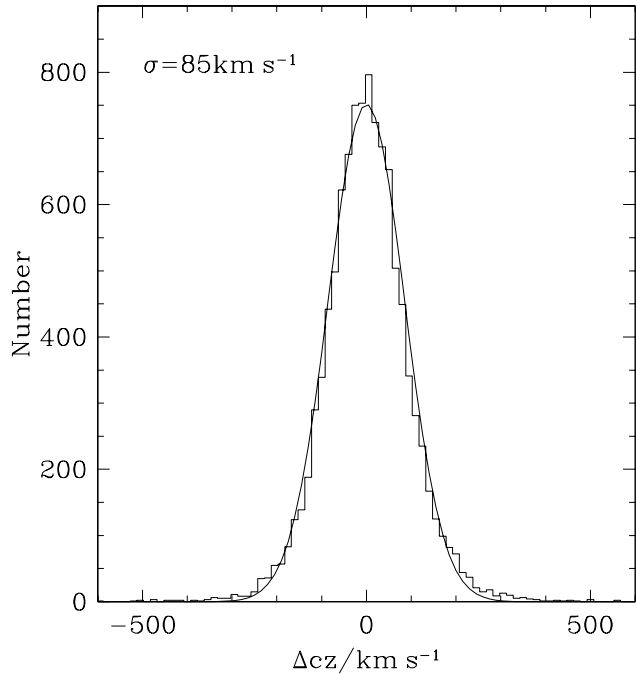


Figure 4. A histogram of the 2dFGRS-SDSS redshift differences for a sample of 10 763 galaxies for which both surveys have measured redshifts with $z > 0.003$. The smooth curve is a gaussian with $\sigma = 85.0 \text{ km s}^{-1}$.

nificantly smaller than the estimate from the spectroscopic sample.

If the SDSS spectroscopic sample were a random sample of the photometric sample then one would expect the two estimates of incompleteness to agree. However, the spectroscopic sample is not a random sample as thresholds have been applied in r-band magnitude and in surface brightness. In addition, close pairs of galaxies are under-represented in the SDSS spectroscopic sample because of the mechanical limits on how close the optical fibres that feed the spectrograph can be placed. If we select a subset of the data using a brighter r-band magnitude limit then we find our incompleteness estimates are not significantly changed. Thus we conclude that the r-band magnitude limit of the spectroscopic sample does not bias our estimates. However, the other two selection effects will bias the estimate. Comparison of the 2dFGRS parent catalogue with deeper wide-area CCD photometry from Pimbblet et al. (2001) and Cross et al. (2001b) has shown that the 2dFGRS misses some low surface brightness galaxies and mis-classifies a fraction of close galaxy pairs. This is a plausible explanation of the difference between the two completeness estimates. We therefore adopt $87 \pm 2\%$ as the 2dFGRS galaxy completeness, consistent with the estimate from the SDSS photometric catalogue. This value is indicated by the horizontal line on Fig. 3.

2.3 Accuracy and Reliability of Redshift Measurements

The 2dFGRS redshift measurements are all assigned a quality flag Q (Colless et al. 2001). For most purposes only

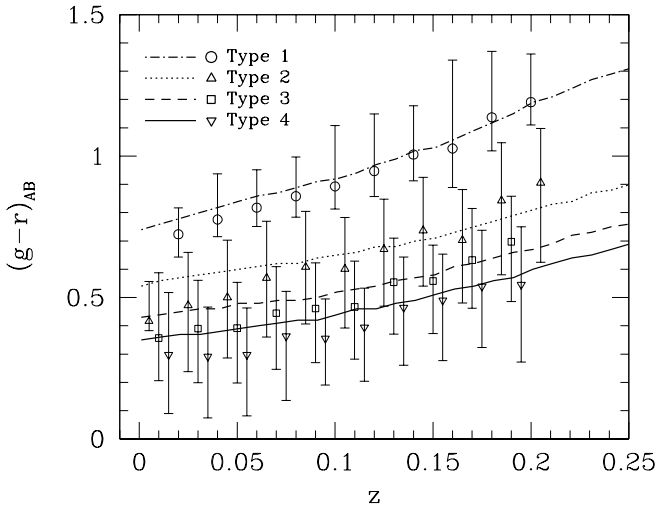


Figure 5. Galaxy $g - r$ colours as a function of redshift. The symbols and error bars show, for each 2dFGRS spectral type, the median, 10 and 90 centiles of the $g - r$ colour distribution, as a function of redshift. The curves are the predictions for model galaxies, computed using the Bruzual & Charlot stellar population synthesis code, whose star formation histories have been selected to reproduce, as closely as possible, the median colour as a function of redshift in each class.

$Q \geq 3$ redshifts are used. From a comparison of repeat observations, Colless et al. (2001) estimated that these have a reliability (defined as the percentage of galaxies whose redshifts are within a 600 km s^{-1} tolerance) of 98.4% and an rms accuracy of 85 km s^{-1} . For higher quality spectra, $Q \geq 4$, these improve to $> 99\%$ and less than 60 km s^{-1} , respectively. Comparison of the 2dFGRS redshifts with the 10 763 galaxies which also have redshift measurements in the SDSS EDR provides a useful check of these numbers. The fraction of objects for which the redshifts differ by more than 600 km s^{-1} is only 1.0%. The redshift differences for the remainder are shown in Fig. 4. This distribution has a width of $\sigma_{68} = 85.0 \text{ km s}^{-1}$ (defined so that $2\sigma_{68}$ spans 68% of the distribution). Taking account of the contribution from the rms error in the SDSS measurements this implies a smaller redshift error than the estimate of Colless et al. (2001). Part of the reason for the difference in these figures is that the SDSS galaxies are on average brighter than typical 2dFGRS galaxies. Also we have only compared measurements when both the SDSS and 2dFGRS redshifts are greater than 0.003. This excludes a small number of 2dFGRS redshifts that are very small due either to contamination of the spectra by moonlight or light from a nearby star. If we further reduce the sample to 10 022 or (8 059) objects by excluding objects whose SDSS and 2dFGRS positions differ by more than 1 or (0.5) arc second then the reliability increases slightly to 99.14 or (99.22)%. This could indicate that some of the discrepant redshifts arise from very close galaxy pairs that are unresolved in the 2dFGRS parent catalogue.

3 k+e-CORRECTIONS

The final ingredient that is required to characterise the selection function of the 2dFGRS is a model describing the change in galaxy magnitudes due to redshifting of the b_J -filter bandpass (k-correction) and galaxy evolution (e-correction). These corrections depend on the galaxy's spectrum and star formation history. As these are correlated, one can parameterize the k+e corrections as functions of the observed spectra.

The 2dFGRS spectra have been classified using a method based on Principal Component Analysis (PCA). A continuous parameter, η , is defined as a linear combination of the first two principal components (Madgwick et al. 2001). The definition of η is such that its value correlates with the strength of absorption/emission features. Galaxies with old stellar populations and strong absorption features have negative values of η , while galaxies with young stellar populations and strong emission lines have positive values. Therefore, we expect the value of η to correlate with the galaxy's k and k+e correction. In Madgwick et al. (2001), the continuous η distribution was divided into four galaxy classes (Type 1: $\eta < -1.4$, Type 2: $-1.4 \leq \eta < 1.1$, Type 3: $1.1 \leq \eta < 3.5$, Type 4: $3.5 \leq \eta$) and the mean k-correction for each type was estimated from the mean spectra of galaxies in each class. A current weakness of this approach is that the overall system response of the 2dF instrument is not well calibrated. This implies that the resulting k-corrections have a systematic uncertainty of around 10% (Madgwick et al. 2001). Due to this problem and also because we wish to estimate k+e corrections and not just k-corrections, we have taken a complementary approach.

The spectrum of any individual galaxy will evolve with time as its star formation rate changes and its stellar population evolves. Consequently, the spectral type of such a galaxy could vary with cosmic time. Therefore, if we want to group the observed galaxies into discrete classes so that the evolution of each class can be described by a single model, we should bin the galaxies in both η and z . Instead, we will bin the galaxies only in η and so not explicitly take account of galaxies which evolve from one spectral class to another. We do this as adopting a more complicated model makes little difference to our results and also it enables us to compare our k-corrections directly with those used in Madgwick et al. (2001).

In Fig. 5, we plot the median observed $g - r$ colour measured from the SDSS EDR data as a function of redshift for each spectral class determined from the 2dFGRS spectra. As expected, we see that galaxy colour and its dependence on redshift correlates with the spectral class. Type 1 galaxies, with the most negative value of η and oldest stellar populations, are reddest and Type 4 are bluest. The curves plotted on Fig. 5 are models constructed using the Bruzual & Charlot (1993; in preparation, see also Liu, Charlot & Graham 1993 and Charlot & Longhetti 2001) stellar population synthesis code. In a manner very similar to that described by Cole et al. (2001), we ran a grid of models each with the same fixed metallicity ($Z = Z_{\odot}/2$) and with a star formation history of the form $\psi(t) \propto \exp(-[t(z) - t(z_f)]/\tau)$, with a set of different timescales, τ . Here, $t(z)$ is the age of the universe at redshift z and the galaxy is assumed to start forming stars at $z_f = 20$. To relate redshift to time, we have

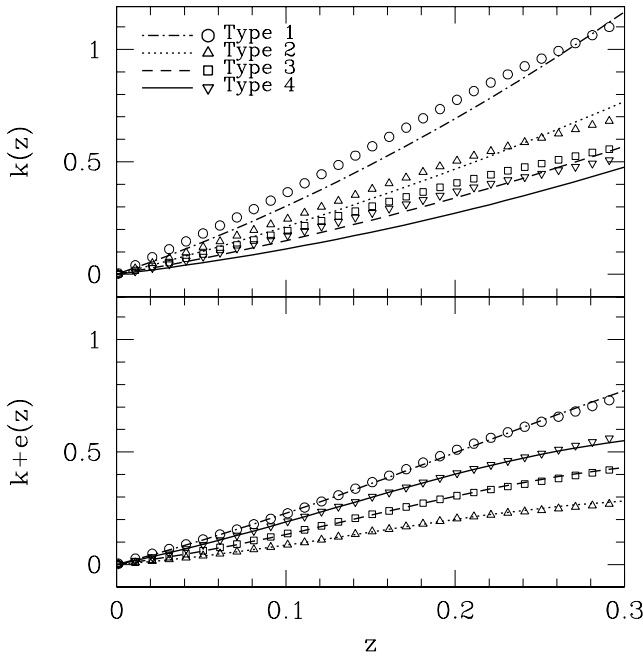


Figure 6. Model k and k+e corrections for each 2dFGRS spectral type. The symbols in the top panel show the k-corrections for four models selected to match the $g-r$ colours as a function of redshift plotted in Fig. 5. The curves show the corresponding k-corrections adopted in Madgwick et al. (2001). The symbols in the lower panel show our model k+e corrections. In this case, the smooth curves are simple analytic fits [Type 1 : $k+e = (2z + 2.8z^2)/(1 + 3.8z^3)$, Type 2: $k+e = (0.6z + 2.8z^2)/(1 + 19.6z^3)$, Type 3: $k+e = (z + 3.6z^2)/(1 + 16.6z^3)$, Type 4: $k+e = (1.6z + 3.2z^2)/(1 + 14.6z^3)$].

assumed a cosmological model with $\Omega_0 = 0.3$, $\Lambda_0 = 0.7$ and Hubble constant $H_0 = 70 \text{ km s}^{-1} \text{ Mpc}^{-1}$. The k and k+e corrections that we derive are only very weakly dependent on these choices.

The models plotted Fig. 5 are the four which best reproduce the observed dependence of the $g-r$ colours with redshift for the four spectral types. They have $\tau = 1, 5, 15$ and 1000 Gyr for Type 1,2,3 and 4 respectively. The models provide a complete description of the galaxy spectral energy distribution and its evolution and so can be used to define k or k+e corrections for each spectral type. These are shown by the symbols in Fig. 6. The Madgwick et al. (2001) k-corrections, shown by the curves in the top panel, are similar but systematically smaller than those we have derived. This systematic difference is comparable to the systematic difference expected given the current uncertainty in the calibration of the 2dF instrument, which the Madgwick et al. (2001) k-corrections rely upon. The bottom panel of Fig. 6 shows our k+e corrections. Simple analytic fits to the k+e correction for each spectral class are given in the figure caption and shown by the smooth curves. Note that the ordering of the k and k+e corrections is not the same. This is because there are competing effects that contribute to the evolutionary correction. As the redshift increases, the age of the stellar population viewed decreases. This effect makes galaxies brighter with increasing redshift, since younger stellar populations have smaller mass-to-light ratios, and also changes the shape of the galaxy spectrum. However, there are fewer

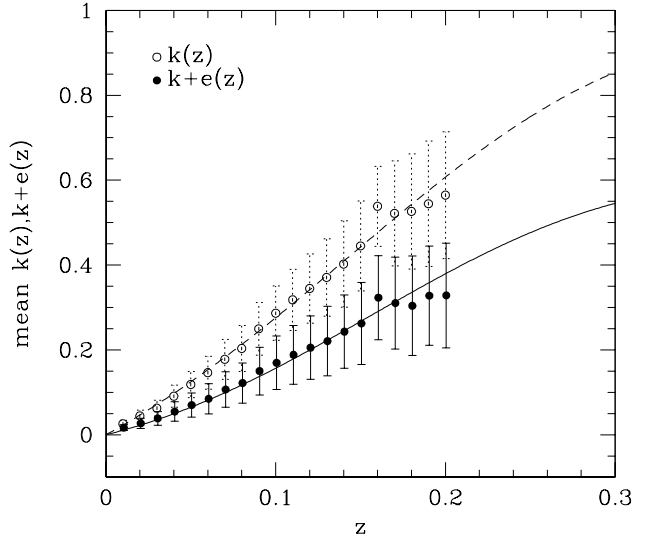


Figure 7. The curves show the fits, $k(z) = (2.2z + 6z^2)/(1 + 15z^3)$ and $k(z) + e(z) = (z + 6z^2)/(1 + 20z^3)$, to the mean k and k+e correction as a function of redshift. The mean corrections at each redshift, shown by the symbols, have been computed as a function of redshift from the known fractions of each spectral type. The error bars show the rms scatter about the mean of these distributions.

stars present at earlier times and this tends to produce a decrease in luminosity with redshift. For galaxies with ongoing star formation (Types 2,3 and 4) these effects can all be significant in determining the overall k+e correction.

It is not possible to assign values of η to all the galaxies in the 2dFGRS. In fact, only galaxies with $z < 0.2$ are classified in this way and approximately 5% of these have spectra with insufficient signal-to-noise to define η . Thus, for some purposes it is necessary to adopt a mean k or k+e correction that can be applied to all galaxies in the survey. In Fig. 7 we show k and k+e corrections averaged over the varying mix of galaxies at each redshift and give simple fitting formulae. We recall that our estimate of the evolutionary correction assumes a cosmological model with $\Omega = 0.3$, $\Lambda = 0.7$ and $H_0 = 70 \text{ km s}^{-1} \text{ Mpc}^{-1}$ in order to relate redshift and look back time. When estimating the galaxy luminosity function for cosmological models with different parameters we retain the same k+e corrections rather than recomputing the best fitting Bruzual & Charlot model. While not being entirely consistent, in practice this makes very little difference to our luminosity function estimates. In section 7, we constrain the uncertainty in k+e correction by comparing luminosity functions estimated in different redshift bins. This enables us to assess the contribution to the error in the luminosity function estimates arising from uncertainties in the k+e corrections.

4 MOCK AND RANDOM CATALOGUES

One of the main purposes of deriving a quantitative description of the survey selection function is to make it possible to construct random (unclustered) and mock (clustered) galaxy catalogues. The random catalogues provide a very flexible description of the selection function and are most

often employed when making estimates of galaxy clustering. The mock catalogues, where the galaxy positions are determined from cosmological N-body simulations, are even more useful. The underlying galaxy clustering and galaxy luminosity function are known for the mock catalogues and so these catalogues can be instrumental in testing and developing codes to estimate these quantities. They also provide a means for assessing the statistical errors due to realistic large scale structure on quantities estimated from the actual redshift survey. Finally, mock catalogues based on different cosmological assumptions provide a direct way to compare clustering statistics for the survey with theoretical predictions. Here, we briefly describe the steps involved in producing the mock catalogues that we use below in sections 6 and 9 and that have been employed earlier in other 2dFGRS analysis papers such as Percival et al. (2001), Norberg et al. (2001a; 2001b). These have been created from the very large “Hubble Volume” simulations carried out by the Virgo consortium (Evrard 1999; Evrard et al. 2001). For more details of the construction of the mock catalogues than are given below see Baugh et al. (2001).

The approach we have taken for generating mock and random catalogues that match the selection and sampling of the 2dFGRS can be broken into two stages. In the first stage, we generate idealized mock catalogues, which have a uniform magnitude limit (somewhat fainter than that of the true survey) and have no errors in the redshift or magnitude measurements. In the second stage, we have the option of introducing redshift and magnitude measurement errors and we sample the catalogue taking into account both its slightly varying magnitude limit and the dependence of the completeness of the redshift catalogue upon position and apparent magnitude. The steps involved in these two stages are outlined below. In practice, in order to have a fast and efficient algorithm, some steps are combined, but the result is entirely equivalent to this simplified description.

(i) The first step in generating a mock catalogue consists of sampling the mass distribution in the N-body simulation so as to produce a galaxy catalogue with the required clustering. We do this by applying one of the simple, ad hoc, biasing schemes described by Cole et al. (1998). We use their Method 2, but with the final density field smoothed with a gaussian with smoothing length $R_S = 2h^{-1}\text{Mpc}$ and with the parameters α and β chosen to match the observed galaxy power spectrum. For this we took the galaxy power spectrum of the APM survey (Baugh & Efstathiou 1993) scaled up in amplitude by 20% to match the amplitude of clustering measured in the 2dFGRS at its median redshift. This results in a fractional rms fluctuation in the density of galaxies in spheres of $8h^{-1}\text{Mpc}$ of $\sigma_8 = 0.87$.

(ii) The second step is to choose the location and orientation of the observer within the simulation. In the mock catalogues used here, this was done by applying certain constraints so that the local environment of the observer resembles that of the Local Group (for details see Baugh et al. 2001).

(iii) We then adopt a Schechter function with $M_{\text{p}_J}^* - 5\log_{10}h = -19.66$, $\alpha = -1.21$ and $\Phi^* = 1.66 \times 10^{-2}h^3\text{Mpc}^{-3}$ as an accurate description of the present day galaxy luminosity function (see Section 7). We combine this with the model of the average k+e correction shown in Fig. 7

and the adopted faint survey magnitude limit to calculate the expected mean comoving space density of galaxies, $\bar{n}(z)$, as a function of redshift.

(iv) We now loop over all the galaxies in the simulation cube that fall within the angular boundaries of the survey and randomly select or reject them so as to produce the required mean $\bar{n}(z)$. In the case of random catalogues, we simply generate randomly positioned points within the boundaries of the survey with spatial number density given by $\bar{n}(z)$.

(v) For each selected galaxy, we generate an apparent magnitude consistent with its redshift, the assumed luminosity function and the faint magnitude limit of the survey.

To degrade these ideal mock catalogues to match the current completeness and sampling of the 2dFGRS requires four more steps.

(i) We perturb the galaxy redshifts by drawing random velocities from a gaussian with $\sigma = 85 \text{ km s}^{-1}$ which is the value estimated in Colless et al. (2001, see also Section 2.3).

(ii) We perturb the galaxy apparent magnitudes, to account for measurement errors, by drawing random magnitude errors from a distribution that accurately fits the histogram of SDSS-2dFGRS magnitude differences shown in Fig. 2d.

(iii) We make use of the map of the survey magnitude limit as a function of position to throw out galaxies that would be too faint to have been included in the actual 2dFGRS parent catalogue.

(iv) The final step incorporates the current level of completeness of the 2dFGRS redshift catalogue. Here, we make use of the maps $R(\theta)$ and $S(\theta, b_J)$, which quantify the completeness of the survey. They are defined in Section 8 of Colless et al. (2001) and summarised in Appendix A. At each angular position, θ , only a fraction, $R(\theta)$, of the redshifts is retained or, taking account of the slight dependence of completeness upon the apparent magnitude, a fraction $S(\theta, b_J)$, which depends upon apparent magnitude, b_J , as well as position, is instead retained.

5 THE 2dFGRS LUMINOSITY FUNCTION FOR DIFFERENT SUB-SAMPLES

The luminosity functions presented here are estimated using fairly standard implementations of the STY (Sandage, Tamman & Yahil 1979) and stepwise maximum likelihood (SWML Efstathiou, Ellis & Peterson 1988) estimators. The only modifications we have made to the methods described in these papers are:

(i) We use the map, $b_J^{\text{lim}}(\theta)$, of the survey magnitude limit to define the apparent magnitude limit for each individual galaxy.

(ii) We use the map of $\mu(\theta)$ to define a weight, $1/c_z(b_J, \mu(\theta))$, for each galaxy (see equation A3) to compensate for the magnitude dependent incompleteness.

Provided the most incomplete 2dF fields are excluded from the sample, then the variation in these weights is small. Slightly more than 76% of the observed 2dF fields have an overall redshift completeness greater than 90%. Here we exclude the few fields for which the redshift completeness is

below 70%. For this sample the mean weight is 1.06 and the rms variation about this is only 0.06. Furthermore, one can make the influence of the weight completely negligible by applying an additional magnitude cut and discarding galaxies fainter than, for example, $b_J = 19.2$.

We have applied both our STY and SWML LF estimators to galaxy samples extracted from the mock galaxy catalogues. In the case of the idealized mock catalogues, not only do the mean estimated luminosity functions agree precisely with the input luminosity function, but also the error estimates agree well with the scatter between the estimates from the 22 different mock catalogues. For the degraded mocks the estimated luminosity functions reproduce well the input luminosity functions convolved with the assumed magnitude errors. It is perhaps also worth noting that we checked that the independently written STY code used in Madgwick et al. (2001) gave identical results when applied to the same sample and assuming the same k-corrections.

Due to the large size of the 2dFGRS the statistical errors in our estimated luminosity functions are extremely small. It is therefore important to verify that systematic errors are well controlled. This is partially demonstrated in Fig. 8, where we compare LF estimates for various subsamples of the 2dFGRS.

For all the samples shown in Fig. 8 we have applied a bright magnitude cut of $b_J > 17$ and assumed an $\Omega_0 = 0.3$, $\Lambda_0 = 0.7$ cosmology. In addition, we have applied various extra cuts to define different subsamples. The smooth curve in each panel of Fig. 8 is a Schechter function (1976) with $M_{b_J}^* - 5\log_{10} h = -19.67$, $\alpha = -1.21$ and $\Phi^* = 1.71 \times 10^{-2} \text{Mpc}^{-3}$. This is the STY estimate for the sample defined by $17 < b_J < 19.2$ and $z < 0.25$. In both the STY and SWML LF estimates, the normalization of the luminosity function is arbitrary. To aid in the comparisons shown in Fig. 8, we have normalized each estimate to produce 153 galaxies per square degree brighter than $b_J = 19.2$ (see Section 6). It can be seen by comparison with the SWML estimates in each panel that the Schechter function is not a good fit at the very bright end. However, it should be borne in mind that in these estimates we have made no attempt to correct for the magnitude measurement errors. Thus, these luminosity functions all represent the true luminosity function convolved with the magnitude measurement errors.

The influence of the assumed k+e correction is investigated in Fig. 8a. Both samples are defined by the limits $17 < b_J < 19.2$ and $z < 0.15$. For one sample, we use the average k+e correction shown in Fig. 7, while for the other, we adopt the spectral class dependent k+e corrections of Fig. 6. The sample to which we apply the class dependent k+e corrections is slightly smaller as a small fraction (5%) of the spectra have insufficient signal-to-noise to enable spectral classification and, in addition, at this stage, not all the spectra have been processed. The upper redshift limit is imposed to avoid the interval where contamination by sky lines causes the spectral classification to be unreliable (Madgwick et al. 2001). We see that, from 2.5 magnitudes fainter than $M_{b_J}^*$ to the brightest magnitudes probed, there is essentially no difference between the two LF estimates. Only for magnitudes fainter than $M_{b_J} - 5\log_{10} h = -17$ does the class dependent estimate fall slightly below the estimate assuming a global k+e correction and then only by an amount comparable to the statistical errors. As this systematic er-

ror is so small, we adopt for all other estimates the global k+e correction which then allows us to use the full redshift sample.

Fig. 8b shows SWML estimates for samples including galaxies with redshifts up to $z = 0.25$. The two estimates compare the results for a sample limited by $b_J < 19.2$ and the sample to the full depth of the 2dFGRS, which has a spatially varying magnitude limit of 19.4 ± 0.1 (see figures 13 and 14 of Colless et al. 2001). The close agreement between the two indicates that no significant bias or error has been introduced by taking account of the varying magnitude limit and including the correction for the magnitude dependent incompleteness.

The remaining panels of Fig. 8 all use samples limited by $b_J < 19.2$, but essentially identical results are found if the samples are extended to the full depth of the survey. Fig. 8c compares the LF estimates from the spatially separated SGP and NGP regions of the 2dFGRS. Brighter than $M_{b_J}^* - 5\log_{10} h = -17.5$, the two regions yield luminosity functions with identical shapes. Note that both luminosity functions have been normalized to produce 153 galaxies per square degree brighter than $b_J = 19.2$, rather than to the actual galaxy number counts in each region. This good agreement suggests that any systematic offset in zeropoint of the magnitude scale in the two disjoint regions is very small. If one allows an offset between the zeropoints of the NGP and SGP magnitude scales, then comparing the bright ends of these two luminosity functions ($M_{b_J} - 5\log_{10} h < -17.5$) constrains this offset to the rather small value 0.014 ± 0.01 . Fainter than $M_{b_J} - 5\log_{10} h = -17.5$ the two estimates differ systematically to a small but significant degree. We return to this difference briefly in Section 7.

Fig. 8d compares results from samples split by redshift. Here, the combined effect of the redshift and apparent magnitude limits results in estimates that only span a limited range in absolute magnitude. To normalize these luminosity functions we extrapolated the estimates using their corresponding STY Schechter function estimates. The two luminosity functions agree well in the overlapping magnitude range and also agree well with the full samples shown in the other panels. This demonstrates that the evolution of the luminosity function is consistent with the k+e-correction model we have adopted. Since we apply k+e corrections, the luminosity function we estimate is always that at $z = 0$.

The final two panels in Fig. 8 examine luminosity functions estimated from bright subsamples of the 2dFGRS. Fig. 8e shows an estimate for galaxies brighter than $b_J = 18.5$ and Fig. 8f for galaxies brighter than $b_J = 18.0$. The statistical errors in the estimates from these smaller samples are significantly larger. Nevertheless, the luminosity functions agree well, on average, with those from the deeper samples.

6 GALAXY NUMBER COUNTS

In the previous section we have demonstrated that the shape of the 2dF galaxy luminosity function, brighter than $M_{b_J} - 5\log_{10} h < -17$, is robust to variations in the sample selection and assumed k+e corrections. We have not yet addressed the issue of normalization and its uncertainty; we simply normalized all the estimates to produce 153 galax-

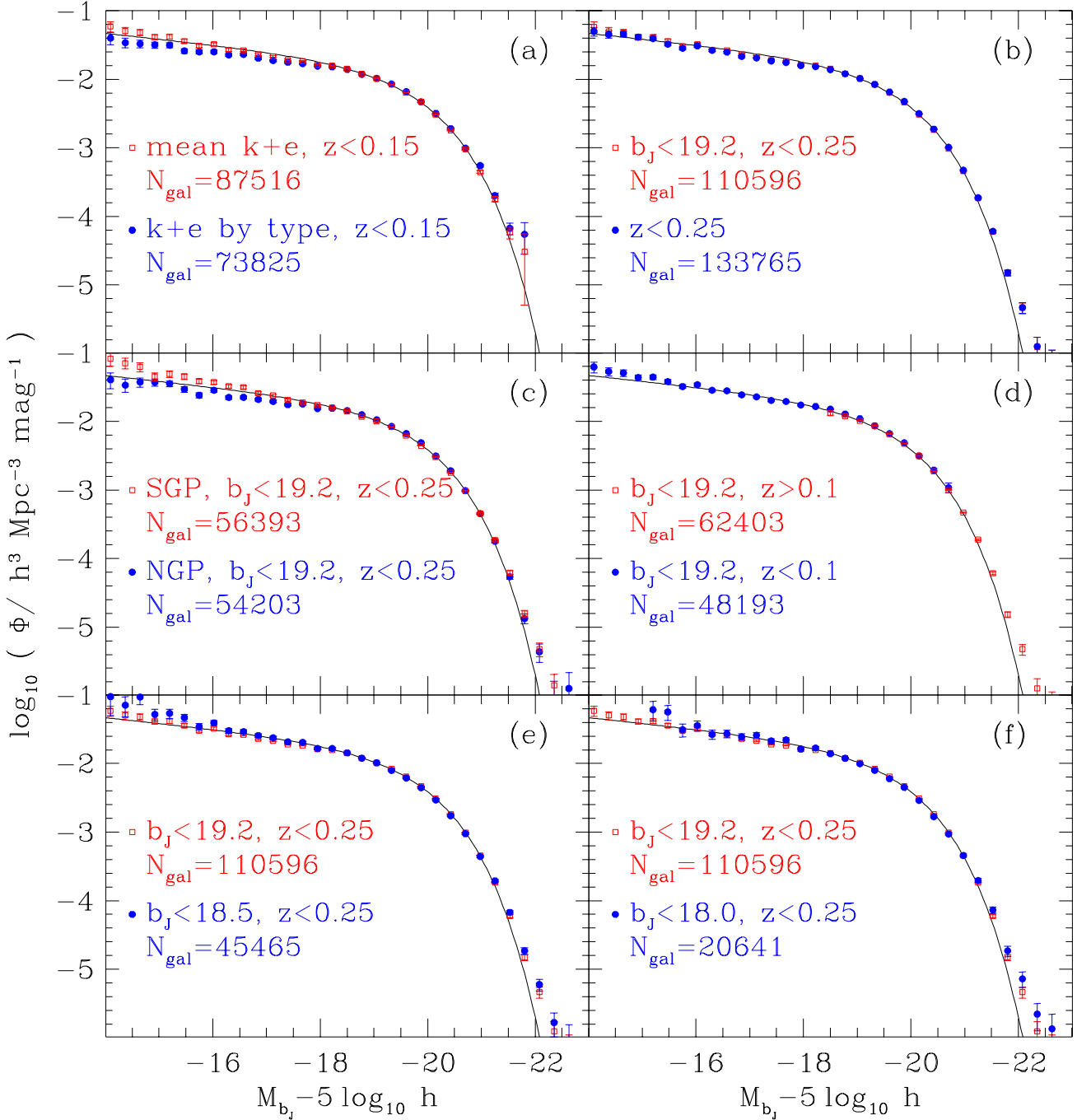


Figure 8. Luminosity functions for different subsamples of the 2dFGRS data. The smooth curve in each panel is a Schechter function with $M_{b_J}^* - 5 \log_{10} h = -19.67$, $\alpha = -1.21$ and $\Phi^* = 1.71 \times 10^{-2} h^3 \text{ Mpc}^{-3}$. This is the STY estimate for the sample defined by $17 < b_J < 19.2$ and $z < 0.25$ and computed using the average k+e correction shown in Fig. 7. This curve is reproduced in each panel as a fiducial reference. In each panel, the points and error bars show SWML LF estimates for two different subsets of the 2dFGRS as indicated by the selection criteria given in each legend (see text for details). Also indicated on each panel is the number of galaxies in each sample. An $\Omega_0 = 0.3$, $\Lambda_0 = 0.7$ cosmology is assumed and the luminosity functions have been normalized to produce 153 galaxies per square degree brighter than $b_J = 19.2$.

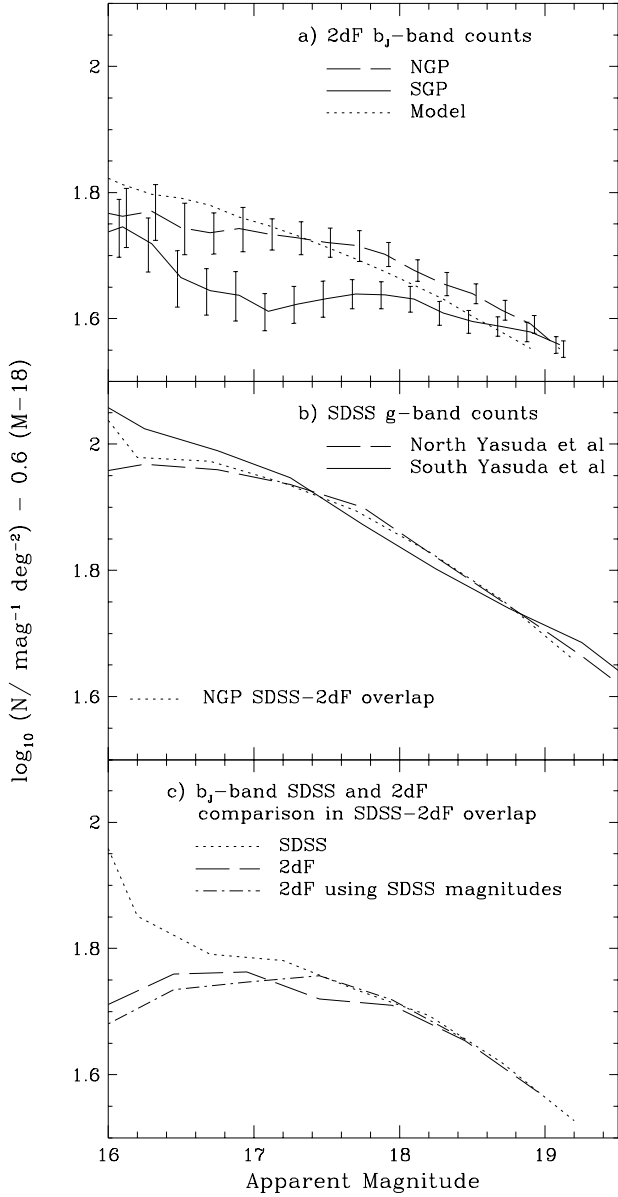


Figure 9. The 2dFGRS and SDSS galaxy number counts in the b_J and g -bands. In each panel we plot the logarithm of the number of galaxies per unit apparent magnitude after subtraction of a Euclidean model. This enables the ordinate to be expanded so that small differences in the counts are visible. The upper panel shows the 2dFGRS b_J -band counts separately in the NGP and SGP regions. The error bars show the rms variation we expect due to large scale structure, estimated from our 22 mock catalogues. The middle panel compares the published SDSS g -band counts of Yasuda et al. (2001) and our own estimate of the SDSS counts in the area which overlaps with the 2dFGRS NGP region. The bottom panel compares, in the overlap region, SDSS and 2dFGRS b_J -band counts.

ies per square degree brighter than $b_J = 19.2$. We now investigate the uncertainty in this normalization due to both large scale structure and the uncertainty in systematic corrections.

The upper panel in Fig. 9 shows the 2dFGRS galaxy b_J -band number counts in the NGP and SGP. In this figure

we have subtracted a Euclidean model from the counts to enable the ordinate to be expanded so that small differences are visible. These are counts of objects in the 2dFGRS parent catalogue (after the removal of the merged images that did not form part of the 2dFGRS target list) multiplied by a factor of $1/(1.054 \times 0.87) = 1.09$ to take account of the stellar contamination (5.4%) and incompleteness (13%) discussed in Section 2.2. While these numbers are derived from a comparison with the SDSS EDR we note that they are very comparable to the original estimates given by Maddox et al. (1990a). The error bars placed on the measured counts are the rms scatter seen in our 22 mock catalogues and provide an estimate of the variation expected due to large scale structure. The dotted curve is the mean number counts in the mocks and corresponds to the expectation for a homogeneous universe.

It has long been known that the galaxy counts in the APM catalogue are steeper than model predictions for a homogeneous universe (Maddox et al. 1990). As we have subtracted the Euclidean slope this manifests itself in Fig. 9 as a shallower slope for the SGP curve than the model prediction shown by the dotted curve. The model assumes $\Omega_0 = 0.3$, $\Lambda_0 = 0.7$, the luminosity function estimated in the previous section and the mean $k+e$ -correction estimated in Section 3. The NGP counts are greater than those in the SGP throughout the range $16 < b_J < 19$ and are also slightly steeper than the model prediction (i.e. shallower in Fig. 9), although the difference is not as extreme as for the SGP. The $1-\sigma$ error bars determined from the mock catalogues show that deviations from the homogeneous model prediction such as those shown by the NGP should be common. The SGP counts are harder to reconcile with the model, but it should be borne in mind that even on quite large scales the galaxy density field is non-gaussian and so $1-\sigma$ error bars do not fully quantify the expected variation.

To normalize our estimates of the galaxy luminosity function we use the cumulative count of galaxies per square degree brighter than $b_J = 19.2$. In the 740 deg^2 of the NGP strip this is 158.6 ± 6.3 , where the error is again the rms from the mock catalogues. The corresponding numbers for the 1094 deg^2 SGP strip are 147.9 ± 6.3 and, for the combined 1841 deg^2 , 153 ± 4.5 . The NGP and SGP number counts differ by 7%, but this is reasonably common in the mock catalogues.

The middle panel in Fig. 9 shows SDSS g -band counts (this being the SDSS band closest to b_J). We show both the published SDSS counts from Yasuda et al. (2001) and our own estimate from the EDR data in the region in which it overlaps with the 2dFGRS NGP strip. The very accurate agreement between the published northern counts and our estimate from the EDR data demonstrates that the simple star-galaxy classification criterion we have used works well fainter than $g = 16.5$ and that we have correctly estimated the area of the overlap between the SDSS EDR and the NGP region of the 2dFGRS. The Yasuda et al. (2001) counts are accurate to brighter magnitudes as they utilise a more sophisticated star-galaxy separation algorithm supplemented by visual classification.

The lower panel of Fig. 9 compares SDSS and 2dFGRS b_J counts within the approximately 173 deg^2 area of overlap of the two datasets. Here, we have estimated b_J from the SDSS Petrosian magnitudes using equation 1, but also

including explicitly the 0.058 magnitude zeropoint offset we measured in Section 2.1. We see that between $18 < b_J < 19$, the 2dFGRS and SDSS number counts agree very accurately. In this area the cumulative count of galaxies per square degree brighter than $b_J = 19.2$ is 160, 5% higher than the average over the ten times larger area covered by the combined NGP+SGP 2dFGRS strips. Between $17 < b_J < 18$ the 2dFGRS counts are approximately 8% below the SDSS counts. Brighter than $b_J = 17$ the difference increases rapidly, but this is due to stellar contamination in our SDSS sample as can be seen by reference to the middle panel of Fig. 9. Interestingly if we compute the counts for the 2dFGRS objects, but using the magnitudes derived from the SDSS data then there is slightly better agreement between 2dFGRS and SDSS at $b_J \approx 17.5$.

We conclude from this comparison that in the 173 deg^2 region of overlap, the 2dFGRS counts (corrected using the standard estimates of stellar contamination and incompleteness) are in good agreement with the SDSS counts fainter than $b_J = 17$, but are 5% higher than those averaged over the full area of the 2dFGRS. The $1 - \sigma$ statistical error estimated from the mock catalogues for an area this size is 4.8%. Over the full area, we find 153 galaxies per square degree brighter than $b_J = 19.2$ with a $1-\sigma$ statistical error, estimated from mock catalogues, of just 3%.

7 THE NORMALIZED 2dFGRS LUMINOSITY FUNCTION

We now use the number counts to normalize our LF estimates. In the upper panel of Fig. 10 we present two independent estimates of the galaxy luminosity function, from the NGP and SGP regions. Here, the LF estimate in each region is normalized by its own galaxy number counts. Thus, the two estimates are independent and the differences between them provide an estimate of the statistical errors. These can be compared with the plotted SWML errors, but note should be taken that the SWML errors do not take account of the uncertainty in the normalization of the luminosity function. For these two estimates, the mock catalogues indicate that the contribution to the uncertainty of the normalization from large scale structure is about 4%. Also of importance is the uncertainty in the incompleteness corrections. We have corrected assuming a global 13% incompleteness in the 2dFGRS photometric catalogue and the uncertainty in this adds, in quadrature, approximately 2% to the normalization uncertainty (see Section 2.1). An indication of this uncertainty is given by the vertical error bar plotted in the upper right of each panel of Fig. 10, which, for clarity, shows the $\pm 3\sigma$ range. If this is added in quadrature to the SWML errors, then one finds that the differences between the NGP and SGP estimates are entirely consistent except for magnitudes fainter than $M_{b_J} - 5\log_{10} h = -17.5$.

At the faint end, the SGP LF is slightly steeper than that estimated from the NGP. This may reflect genuine spatial variations in the galaxy luminosity function as this faint portion of the luminosity function is determined from a very local volume. Such variations are perhaps to be expected given the results of Norberg et al. (2001a; 2001b) that show that galaxies of different luminosity have systematically different clustering properties. The faint end of the luminosity

function may also be affected by incompleteness in the 2dFGRS. We have corrected the luminosity function assuming that the incompleteness is independent of absolute magnitude. However, from the joint analysis of the 2dFGRS and the much deeper MGC catalogue by Cross et al. (2001b), we know that part of the incompleteness is due to the 2dFGRS preferentially missing low surface brightness galaxies. The correlation between absolute magnitude and surface brightness (Ferguson & Binggeli 1994; Driver 1999) then implies that low luminosity galaxies are underrepresented. The work of Cross & Driver (2001) (see also Cross et al. 2001b) suggests that this only becomes important fainter than $M_{b_J} - 5\log_{10} h = -16.0$.

There are two other significant contributions to the uncertainty in the galaxy luminosity function on an absolute scale. The first of these is the zeropoint of the photometry which has an accuracy of ± 0.04 magnitudes. The size of this uncertainty is indicated by the horizontal error bar plotted in the upper right of each panel of Fig. 10, which shows the $\pm 3\sigma$ range. The second important contribution is the uncertainty in the appropriate evolutionary correction. Our estimates of the galaxy luminosity function are at redshift $z = 0$ and so rely on an accurate model of the $k+e$ corrections to transform the measured luminosities, which have a median redshift of $z_{\text{med}} \approx 0.1$, to present day values. The $k+e$ -corrections we use are accurately constrained by the SDSS g-r colours, but are nevertheless model dependent at some level. To gauge the uncertainty in the luminosity function due to this uncertainty we made SWML LF estimates using $k+e$ -corrections that were increased or decreased by some factor compared to our standard model. We then constrained this factor by requiring statistical consistency between LF estimates made separately for the data above and below $z = 0.1$. The results of this test for the standard $k+e$ -correction model were shown in Fig. 8d, where it can be seen that the two luminosity functions match accurately. We find that if the $k+e$ -corrections are increased or decreased by 18%, then the position of the break in the luminosity function between the high and low redshift samples differs by 1σ (as determined using the SWML errors). Taking this as an estimate of the uncertainty in the $k+e$ correction we find that the corresponding uncertainties in the luminosity function parameters are $\Delta\alpha = 0.02$, $\Delta M^* = 0.06$, and $\Delta\Phi^*/\Phi^* = 3\%$. The variations in M^* and Φ^* are strongly correlated as for a given value of M^* , Φ^* is determined using the normalization constraint provided by the number counts. This contribution to the uncertainty in the LF estimates is indicated by the slanted error bar plotted in the upper right of each panel of Fig. 10, which again shows the $\pm 3\sigma$ range.

The lower panel of Fig. 10 combines the SGP and NGP data to give our best estimate of the b_J -band galaxy luminosity function assuming an $\Omega_0 = 0.3$ and $\Lambda_0 = 0.7$ cosmology. The points with $\pm 1\sigma$ error bars show the SWML estimate. Also shown are two Schechter functions, whose parameter values are indicated in the legend. The first is a simple STY estimate of the 2dFGRS LF, while the second is obtained by fitting the SWML estimate by a Schechter function convolved with the distribution of magnitude measurement errors estimated from Fig. 2. We see that deconvolving the effect of the magnitude errors causes only a small reduction in L^* and Φ^* . We also see that this function convolved

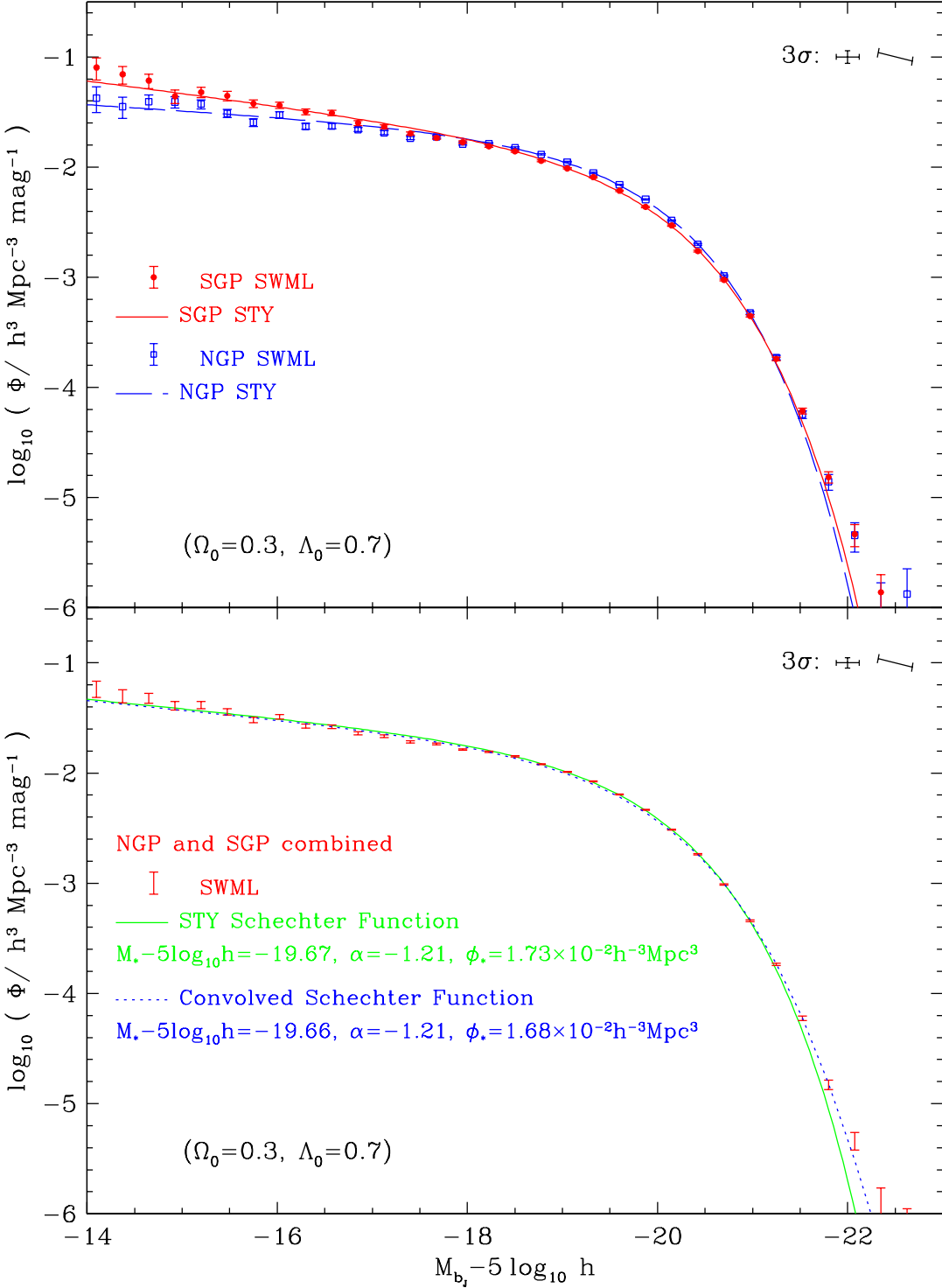


Figure 10. The upper panel shows two independent estimates of the $z = 0$ galaxy luminosity function, from the NGP and SGP regions. The lower panel shows the combined NGP+SGP estimate, normalized to the mean NGP+SGP number counts. The symbols show SWML estimates with $\pm 1\sigma$ error bars and the smooth solid curves STY Schechter function estimates. The dotted curve in the lower panel is the fit to the SWML LF obtained using a Schechter function convolved with the distribution of magnitude measurement errors. The parameters of the Schechter functions are given in the legend. The error bars shown in the upper right of each panel are 3σ (for clarity) errors showing the additional uncertainty in the normalization (vertical), in the photometric zeropoint (horizontal) and in the k+e-corrections (slanted). These three sources of error are all independent, but affect each data point in the luminosity function coherently. Here, and in all our plots, an $\Omega_0 = 0.3$ and $\Lambda_0 = 0.7$ cosmology is assumed. The values of the SWML estimate are given in Table 1 and the parameters of the deconvolved Schechter function fits are given in Table 2, along with estimates for alternative choices of the cosmological parameters.

Table 1. The stepwise maximum likelihood (SWML) estimates of the 2dFGRS $z = 0$ galaxy luminosity function for three assumed cosmological models. The quoted errors do not take account of uncertainty in the normalization, the photometric zeropoint or uncertainty in the appropriate evolutionary correction (see Section 6). Also these estimates are not deconvolved for the effect of random magnitude measurement errors.

$M_{b_J} - 5\log_{10} h$	$\Omega_0 = 0.3, \Lambda_0 = 0.7$	$\Omega_0 = 1, \Lambda_0 = 0$	$\Omega_0 = 0.3, \Lambda_0 = 0$
	$\Phi/h^3 \text{Mpc}^{-3}$	$\Phi/h^3 \text{Mpc}^{-3}$	$\Phi/h^3 \text{Mpc}^{-3}$
-13.275	$(9.275 \pm 4.779) \times 10^{-2}$	$(1.153 \pm 0.592) \times 10^{-1}$	$(1.146 \pm 0.590) \times 10^{-1}$
-13.550	$(5.600 \pm 1.927) \times 10^{-2}$	$(6.584 \pm 2.250) \times 10^{-2}$	$(6.420 \pm 2.197) \times 10^{-2}$
-13.825	$(5.913 \pm 1.350) \times 10^{-2}$	$(6.747 \pm 1.533) \times 10^{-2}$	$(6.521 \pm 1.483) \times 10^{-2}$
-14.100	$(5.847 \pm 1.003) \times 10^{-2}$	$(6.440 \pm 1.108) \times 10^{-2}$	$(5.767 \pm 1.024) \times 10^{-2}$
-14.375	$(5.014 \pm 0.693) \times 10^{-2}$	$(5.800 \pm 0.787) \times 10^{-2}$	$(5.714 \pm 0.772) \times 10^{-2}$
-14.650	$(4.793 \pm 0.510) \times 10^{-2}$	$(5.386 \pm 0.566) \times 10^{-2}$	$(5.158 \pm 0.547) \times 10^{-2}$
-14.925	$(4.116 \pm 0.367) \times 10^{-2}$	$(4.609 \pm 0.406) \times 10^{-2}$	$(4.506 \pm 0.398) \times 10^{-2}$
-15.200	$(4.153 \pm 0.302) \times 10^{-2}$	$(4.776 \pm 0.340) \times 10^{-2}$	$(4.525 \pm 0.326) \times 10^{-2}$
-15.475	$(3.602 \pm 0.233) \times 10^{-2}$	$(4.076 \pm 0.258) \times 10^{-2}$	$(3.926 \pm 0.250) \times 10^{-2}$
-15.750	$(3.046 \pm 0.174) \times 10^{-2}$	$(3.463 \pm 0.193) \times 10^{-2}$	$(3.338 \pm 0.187) \times 10^{-2}$
-16.025	$(3.244 \pm 0.155) \times 10^{-2}$	$(3.685 \pm 0.171) \times 10^{-2}$	$(3.545 \pm 0.166) \times 10^{-2}$
-16.300	$(2.677 \pm 0.117) \times 10^{-2}$	$(3.080 \pm 0.130) \times 10^{-2}$	$(2.935 \pm 0.125) \times 10^{-2}$
-16.575	$(2.642 \pm 0.102) \times 10^{-2}$	$(3.008 \pm 0.113) \times 10^{-2}$	$(2.866 \pm 0.109) \times 10^{-2}$
-16.850	$(2.303 \pm 0.078) \times 10^{-2}$	$(2.653 \pm 0.086) \times 10^{-2}$	$(2.545 \pm 0.084) \times 10^{-2}$
-17.125	$(2.154 \pm 0.062) \times 10^{-2}$	$(2.479 \pm 0.067) \times 10^{-2}$	$(2.393 \pm 0.066) \times 10^{-2}$
-17.400	$(1.914 \pm 0.045) \times 10^{-2}$	$(2.141 \pm 0.048) \times 10^{-2}$	$(2.055 \pm 0.047) \times 10^{-2}$
-17.675	$(1.841 \pm 0.037) \times 10^{-2}$	$(2.092 \pm 0.040) \times 10^{-2}$	$(2.002 \pm 0.039) \times 10^{-2}$
-17.950	$(1.635 \pm 0.029) \times 10^{-2}$	$(1.899 \pm 0.031) \times 10^{-2}$	$(1.819 \pm 0.030) \times 10^{-2}$
-18.225	$(1.567 \pm 0.023) \times 10^{-2}$	$(1.788 \pm 0.025) \times 10^{-2}$	$(1.705 \pm 0.024) \times 10^{-2}$
-18.500	$(1.423 \pm 0.019) \times 10^{-2}$	$(1.592 \pm 0.020) \times 10^{-2}$	$(1.535 \pm 0.019) \times 10^{-2}$
-18.775	$(1.206 \pm 0.014) \times 10^{-2}$	$(1.343 \pm 0.015) \times 10^{-2}$	$(1.297 \pm 0.014) \times 10^{-2}$
-19.050	$(1.028 \pm 0.011) \times 10^{-2}$	$(1.145 \pm 0.011) \times 10^{-2}$	$(1.100 \pm 0.011) \times 10^{-2}$
-19.325	$(8.379 \pm 0.081) \times 10^{-3}$	$(9.030 \pm 0.084) \times 10^{-3}$	$(8.864 \pm 0.083) \times 10^{-3}$
-19.600	$(6.423 \pm 0.060) \times 10^{-3}$	$(6.906 \pm 0.063) \times 10^{-3}$	$(6.714 \pm 0.062) \times 10^{-3}$
-19.875	$(4.657 \pm 0.045) \times 10^{-3}$	$(4.767 \pm 0.046) \times 10^{-3}$	$(4.750 \pm 0.046) \times 10^{-3}$
-20.150	$(3.078 \pm 0.032) \times 10^{-3}$	$(2.986 \pm 0.032) \times 10^{-3}$	$(3.025 \pm 0.032) \times 10^{-3}$
-20.425	$(1.837 \pm 0.022) \times 10^{-3}$	$(1.688 \pm 0.021) \times 10^{-3}$	$(1.782 \pm 0.022) \times 10^{-3}$
-20.700	$(9.789 \pm 0.139) \times 10^{-4}$	$(8.435 \pm 0.136) \times 10^{-4}$	$(8.812 \pm 0.135) \times 10^{-4}$
-20.975	$(4.567 \pm 0.085) \times 10^{-4}$	$(3.542 \pm 0.083) \times 10^{-4}$	$(4.018 \pm 0.085) \times 10^{-4}$
-21.250	$(1.836 \pm 0.050) \times 10^{-4}$	$(1.159 \pm 0.046) \times 10^{-4}$	$(1.356 \pm 0.047) \times 10^{-4}$
-21.525	$(5.960 \pm 0.282) \times 10^{-5}$	$(3.475 \pm 0.260) \times 10^{-5}$	$(4.166 \pm 0.263) \times 10^{-5}$
-21.800	$(1.486 \pm 0.144) \times 10^{-5}$	$(9.133 \pm 1.395) \times 10^{-6}$	$(1.147 \pm 0.143) \times 10^{-5}$
-22.075	$(4.631 \pm 0.838) \times 10^{-6}$	$(2.999 \pm 0.860) \times 10^{-6}$	$(3.661 \pm 0.857) \times 10^{-6}$
-22.350	$(1.249 \pm 0.469) \times 10^{-6}$	$(6.532 \pm 4.576) \times 10^{-7}$	$(5.022 \pm 3.519) \times 10^{-7}$
-22.625	$(7.048 \pm 4.042) \times 10^{-7}$	$(5.592 \pm 5.577) \times 10^{-7}$	$(3.735 \pm 3.727) \times 10^{-7}$

Table 2. Schechter function fits to the 2dFGRS galaxy luminosity function for three assumed cosmological models. The parameters specify the Schechter functions which, when convolved with the apparent magnitude measurement errors, give the best fits to the SWML estimate of the 2dFGRS galaxy luminosity function. The last column lists the integrated luminosity density in solar units ($M_{b_J}^{\odot} = 5.3$). The contributions to the quoted errors on the values of the Schechter function parameters have been divided into four distinct categories: a) The errors directly from STY maximum likelihood estimate of $M_{b_J}^*$ and α . Once combined with the normalization constraint these induce a corresponding uncertainty in Φ^* . b) The contribution due to the uncertainty in the $k+e$ corrections. c) The uncertainty in the photometric zeropoint. d) The uncertainty in the normalization due to large scale structure and residual uncertainty in the incompleteness correction. If one is interested in the absolute error in the luminosity function these errors should be added in quadrature.

Ω_0	Λ_0	$M_{b_J}^* - 5\log_{10} h$	α	$\Phi^*/h^3 \text{Mpc}^{-3}$	$\rho_L/hL_{\odot} \text{Mpc}^{-3}$
0.3	0.7	$-19.66 \pm 0.006^a \pm 0.06^b \pm 0.04^c$	$-1.21 \pm 0.01^a \pm 0.02^b$	$(1.68 \pm 0.015^a \pm 0.05^b \pm 0.06^d) \times 10^{-2}$	$(1.90 \pm 0.18) \times 10^8$
1	0	$-19.48 \pm 0.006^a \pm 0.06^b \pm 0.04^c$	$-1.18 \pm 0.01^a \pm 0.02^b$	$(2.15 \pm 0.020^a \pm 0.06^b \pm 0.08^d) \times 10^{-2}$	$(2.01 \pm 0.19) \times 10^8$
0.3	0	$-19.54 \pm 0.006^a \pm 0.06^b \pm 0.04^c$	$-1.19 \pm 0.01^a \pm 0.02^b$	$(1.96 \pm 0.019^a \pm 0.06^b \pm 0.07^d) \times 10^{-2}$	$(1.97 \pm 0.19) \times 10^8$

with the errors (dotted curve) produces a good match to the SWML estimate. Thus, there is little evidence for the underlying galaxy luminosity function differing significantly from the Schechter function form.

The numerical values of these estimates are listed in

Tables 1 and 2, along with estimates for alternative cosmologies. Note that the SWML estimates refer to the observed luminosity function, which is distorted by random magnitude measurement errors. In contrast, the Schechter function parameters listed in Table 2 refer to the underlying

ing galaxy luminosity function deconvolved for the effect of magnitude measurement errors. In Table 2 we have broken down the errors on the Schechter function parameters into three components. The first is the statistical error returned by the STY maximum likelihood method. The large number of galaxies used in our estimates makes this statistical error very small and so it is never the dominant contribution to the overall error. The second error is our estimate of the error induced by the uncertainty in the k+e-corrections. This is the dominant contribution to the error in α and also a significant contributor to the errors in M^* and Φ^* . The third error given for M^* in Table 2 is due to the current uncertainty in the 2dFGRS photometric zeropoint. This will be reduced when more calibrating CCD photometry is available. The third error given for Φ^* is due to the uncertainty in the galaxy number counts and has contributions from large-scale structure (3%) and from the uncertainty in the incompleteness corrections (2%). To determine the overall errors on an absolute scale these contributions should all be added in quadrature. For a complete description of the errors one also needs to consider the correlations between the different parameters. For both the contribution to the errors coming from the uncertainty in the STY parameter estimation and from the uncertainty in the k+e-correction a steeper faint end slope, α , correlates with brighter M^* . This, in turn, is correlated with Φ^* as the number count constraint implies that a brighter M^* will produce a lower Φ^* . In each case the correlation coefficient is large, $R \approx 0.8$. The uncertainty in the photometric zeropoint effects only M^* , while the uncertainty in the number count constraint effects only Φ^* . This reduces the correlation between the parameter estimates. The final column in Table 2 lists the implied $z = 0$ luminosity density in solar units. The error quoted on this quantity was computed by propagating all the previously mentioned errors.

The Schechter function parameters listed in Table 2 for the $\Omega_0 = 0.3$, $\Lambda_0 = 0.7$ cosmology differ slightly from those in Madgwick et al. (2001). This is to be expected as the Madgwick et al. luminosity functions are not corrected for evolution. That paper focused on the dependence of the luminosity function on spectral type. Adopting the average k-correction of Madgwick et al. and using this in place of our k+e-correction on our larger sample (the Madgwick et al. sample is truncated at $z = 0.15$), we find luminosity function parameters very close to those of Madgwick et al. (2001). The remaining, very small differences are accounted for by slightly differing models for the magnitude errors and the adopted normalizations.

8 COMPARISON WITH INDEPENDENT LUMINOSITY FUNCTION ESTIMATES

In Fig. 11 we compare the STY and SWML estimates of the b_J -band LF from the combined NGP+SGP 2dFGRS sample defined by $17 < b_J < 19.2$ and $z < 0.25$ (shown in Fig 10) with estimates from other surveys. The upper panel compares 2dFGRS with various estimates made from the SDSS. In this comparison we again assume an $\Omega_0 = 0.3$, $\Lambda_0 = 0.7$ cosmology. Blanton et al. (2001) presented an estimate of the b_J -band LF for the case of $\Omega_0 = 1.0$. We do not use this, but instead estimate the b_J -band LF for our adopted

cosmology using the g-band LF computed by Blanton et al. (2001) for the $\Omega_0 = 0.3$, $\Lambda_0 = 0.7$ cosmology and the typical $B - V$ galaxy colour. Using the colour equations of Fukugita et al. (1996), and assuming $b_J = B - \beta(B - V)$, one finds $b_J = g + 0.12 + (0.44 - \beta)(B - V)$ Blanton et al. 2001 assumed $\beta = 0.35$, based on the work of Metcalfe et al. (1995), and contrary to the commonly-used value of $\beta = 0.28$ (Blair & Gilmore 1982). Thus, an estimate of the b_J -band LF can be made by simply taking the g-band estimate and shifting the magnitudes using this equation with $B - V = 0.94$, this being the mean colour measured for galaxies brighter than $b_J = 19$ in the SDSS sample. This procedure can be seen to work quite accurately: when applied to the $\Omega_0 = 1$ g-band LF parameters given in table 2 of Blanton et al. (2001), it reproduces the corresponding b_J parameters given in their Fig. 23. Taking $\beta = 0.35$ and applying this procedure for the $\Omega_0 = 0.3$, $\Lambda_0 = 0.7$ cosmology gives $M_{b_J}^* - 5\log_{10} h = -19.82$, $\alpha = -1.26$ and $\Phi^* = 2.06 \times 10^{-2} h^3 \text{Mpc}^{-3}$. This Schechter function is shown by the long dashed curve in the upper panel of Fig. 11. As discussed by Blanton et al. (2001), this estimate is incompatible with the 2dFGRS estimate and predicts a significantly higher luminosity density than we find.

The short dashed line in the upper panel of Fig. 11, a Schechter function with $M_{b_J}^* - 5\log_{10} h = -19.68$, $\alpha = -1.26$ and $\Phi^* = 1.63 \times 10^{-2} h^3 \text{Mpc}^{-3}$, is the result of making three modifications to the Blanton et al. (2001) curve. First, we have shifted $M_{b_J}^*$ by 0.08 magnitudes as is appropriate if one adopts the Blair & Gilmore (1982) colour equation $b_J = B - 0.28(B - V)$ rather than $b_J = B - 0.35(B - V)$ used by Blanton et al. (2001). The latter is actually ruled out by the empirical relations found by matching the 2dFGRS catalogue with either the EIS or SDSS which are instead consistent with the former. Second, we have shifted $M_{b_J}^*$ by a further 0.058 to take account of the zeropoint offset between the SDSS and 2dFGRS photometry that we found in Section 2.1 (Fig. 2c). Finally, we have reduced Φ^* by 21%, the reduction required for this luminosity function to reproduce the mean 2dFGRS number counts at $b_J = 19.2$ assuming our standard k+e-correction model. We note that Yasuda et al. (2001) also found a value of Φ^* significantly lower than Blanton et al. when they normalized the SDSS g-band luminosity function using the SDSS galaxy counts. The Yasuda et al. estimate is still higher than our value, because although the SDSS counts agree with 2dFGRS in the area of overlap, this smaller area (173deg^2) has a 5% higher density of galaxies than the full area (1841deg^2) covered by the 2dFGRS survey (see Section 6). This modified SDSS Schechter function is in near perfect agreement with the Schechter function estimated from the 2dFGRS.

At the brightest magnitudes, the 2dFGRS SWML estimate is above both the 2dFGRS STY estimate and the modified SDSS Schechter function estimate. As we have seen, the main reason for this is that magnitude measurement errors in the 2dFGRS have a significant effect on the bright end of the luminosity function, but little effect around M^* and fainter. The solid curve surrounded by the shaded region shows the result of convolving the modified SDSS estimate with the model of the 2dFGRS magnitude errors shown in Fig. 2. The shaded region indicates the statistical error on the SDSS estimate and was read off figure 6 of Blanton et al. (2001). Comparing this with the 2dFGRS SWML estimate

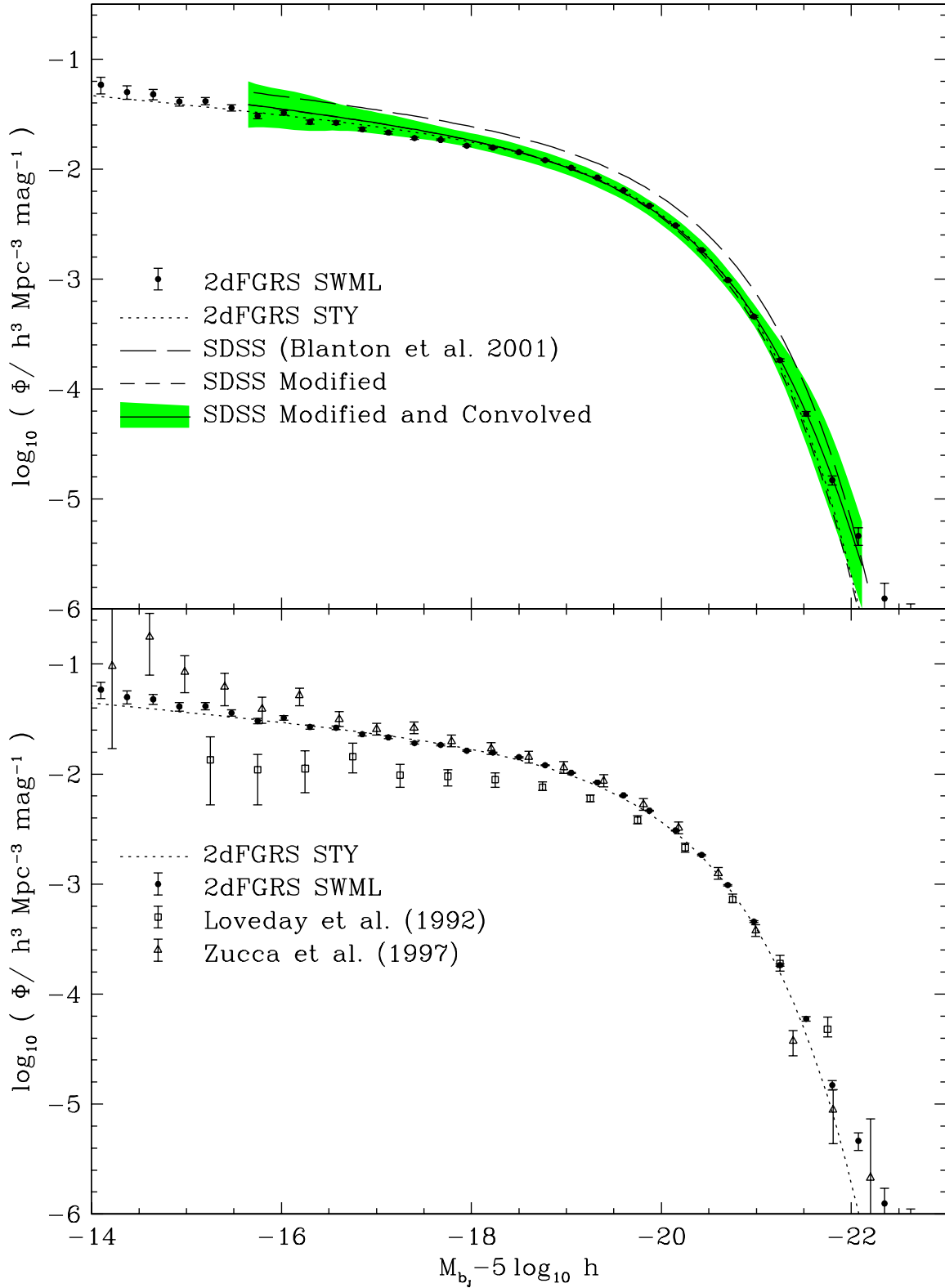


Figure 11. Comparison of the 2dFGRS b_J -band luminosity function with estimates from the SDSS and the earlier estimates of Loveday et al. (1992) and Zucca et al. (1997).

we see that the two are perfectly consistent, with the larger 2dFGRS sample having significantly smaller statistical errors.

We have seen that after taking into account the zero-point photometric offset and the error in the colour equation, the only significant difference between the LF estimates of Blanton et al. (2001) and the 2dFGRS is a difference in Φ^* . This difference arises not because the density of galaxies is higher in SDSS than 2dFGRS (the counts agree to 5%), but because of the different methods used to constrain Φ^* . Blanton et al. used the method of Davis & Huchra (1982) which weights galaxies as a function of redshift in order to obtain a minimum variance estimate of the galaxy density. This method gives more weight to galaxies at high redshift than the method based on normalizing to the counts. It results in a smaller statistical error in the normalization, but at the same time renders the result more dependent on the accuracy of the evolutionary correction. We have seen in Section 7 that, even with the low redshift constraint provided by the galaxy counts, the uncertainty in Φ^* due to the uncertainty in the $k+e$ correction is significant. With the Davis & Huchra weighting this uncertainty becomes dominant. The analysis by Blanton et al. did not take account of evolution – only k -corrections were applied – and this appears to have given rise to an artificially high estimate of Φ^* in the g -band. We conclude that, when normalized in the same way, there is excellent agreement between the SDSS and 2dFGRS luminosity functions and that the dominant remaining uncertainty in the present day b_J -band LF is due to residual uncertainties in evolutionary corrections.

The lower panel of Fig. 11 compares the 2dFGRS result with the earlier estimates of Loveday et al. (1992) and Zucca et al. (1997). We see that the Zucca et al. estimate agrees well with 2dFGRS although it has statistical errors that are much larger. The main difference with the luminosity function of Loveday et al. (1992) is its lower Φ^* . Both estimates are based on catalogues extracted from the APM survey. However, the Loveday et al. sample is much brighter and almost disjoint from the sample analyzed in this paper. As we have seen, the bright galaxy number counts in the SGP drop below model predictions extrapolated from fainter magnitudes (Maddox et al. 1990 and Section 6) and it is therefore not surprising that Loveday found a lower value of Φ^* . Similarly, the flatter faint end slope that they find might be attributed, at least in part, to small volume effects.

9 THE 2dFGRS SELECTION FUNCTION

The luminosity function we have derived, combined with the maps defining the survey magnitude limit (see figure 13 Colless et al. 2001), redshift completeness (see Fig. 1) and μ -parameter (see Fig. A1) specify the complete selection function of the 2dFGRS.[†] It is interesting to compare the red-

[†] The only significant aspects of the 2dFGRS selection function ignored in this description are surface brightness issues (see Cross et al. 2001b) and the undersampling of close galaxy pairs induced by the mechanical limits on the positioning of the optical fibres that feed the 2dF spectrograph. Note that as the 2dF fields overlap, not all close galaxy pairs are missed. We have found that when making estimates of galaxy clustering an accurate way of

shift distribution implied by this selection function with the measured distribution. Note that the luminosity function estimators we employed are insensitive to clustering and so the information contained in the redshift distribution of the galaxies has not been used in determining our model of the selection function.

In Fig. 12 we compare the smooth redshift distribution predicted by our model of the 2dFGRS selection function with the observed distribution. The left-hand panels show the redshift distributions for the full 2dFGRS survey split into the SGP and NGP regions. The right-hand panels show the distributions only for galaxies brighter than $b_J = 18.5$. The dotted lines indicate the rms variation in the redshift histograms found in our 22 mock 2dFGRS catalogues. Gravitational clustering produces a pattern of galaxy clustering that is non-gaussian, composed of voids, walls, filaments and clusters (e.g. see figures 8 to 15 of Cole et al. 1998 for mock 2dFGRS and SDSS cone plots). As a result, the rms variation in the $N(z)$ distribution does not give an adequate description of the variation seen in the mock catalogues. For this reason we show in Fig. 13 two examples of the redshift distributions found in our ensemble of mock catalogues. From these we see that the few large spikes present in the $N(z)$ of the 2dFGRS data are common features in the mock catalogue redshift distributions.

The redshift distribution in the 2dFGRS NGP has a large spike close to the peak of the selection function and otherwise lies within $1-\sigma$ of our smooth selection function. Thus, the density field in the NGP strip looks in no way unusual when compared to the expectation in the standard Λ CDM ($\Omega_0 = 0.3$, $\Lambda_0 = 0.7$) universe. In contrast, the density field in the SGP appears more extreme. Focusing first on the redshift distribution below $z < 0.2$, we see that the observed galaxy density is nearly always below the mean density predicted by the selection function. This behaviour is consistent with the steep APM galaxy number counts, first noted by Maddox et al. (1990), and discussed in Section 6 above. A lower than average galaxy density over such a large range of redshift is certainly an unlikely occurrence. However, as illustrated by the example of the mock SGP plotted in Fig. 13, which in many respects is quite similar to the observed 2dFGRS SGP, comparable variations do occur in the mock Λ CDM catalogues. The two examples plotted in Fig. 13 were not chosen at random, but as we only have 22 mocks to choose from, they do not represent extreme possibilities.

The 2dFGRS SGP strip also appears to show an over-density, relative to the mean implied by the selection function, in the redshift range $0.2 < z < 0.25$. As the volume contributing to this redshift interval is very large, a variation as extreme as this is very unlikely. It therefore seems implausible that this perturbation in $N(z)$ is due solely to large-scale structure. There are some structures at this redshift that contribute to the excess, but even if they are excised the $N(z)$ remains higher than the model. At $z > 0.2$ the only

dealing with this incompleteness is to assign the weight of the missed galaxies to neighbouring galaxies with redshifts. We typically distribute the weight of a missed galaxy between its 10 nearest neighbours and find that this produces accurate clustering estimates on scales greater than 1.5 arcmin or $\sim 0.2h^{-1}\text{Mpc}$ (Norberg et al. 2001c).

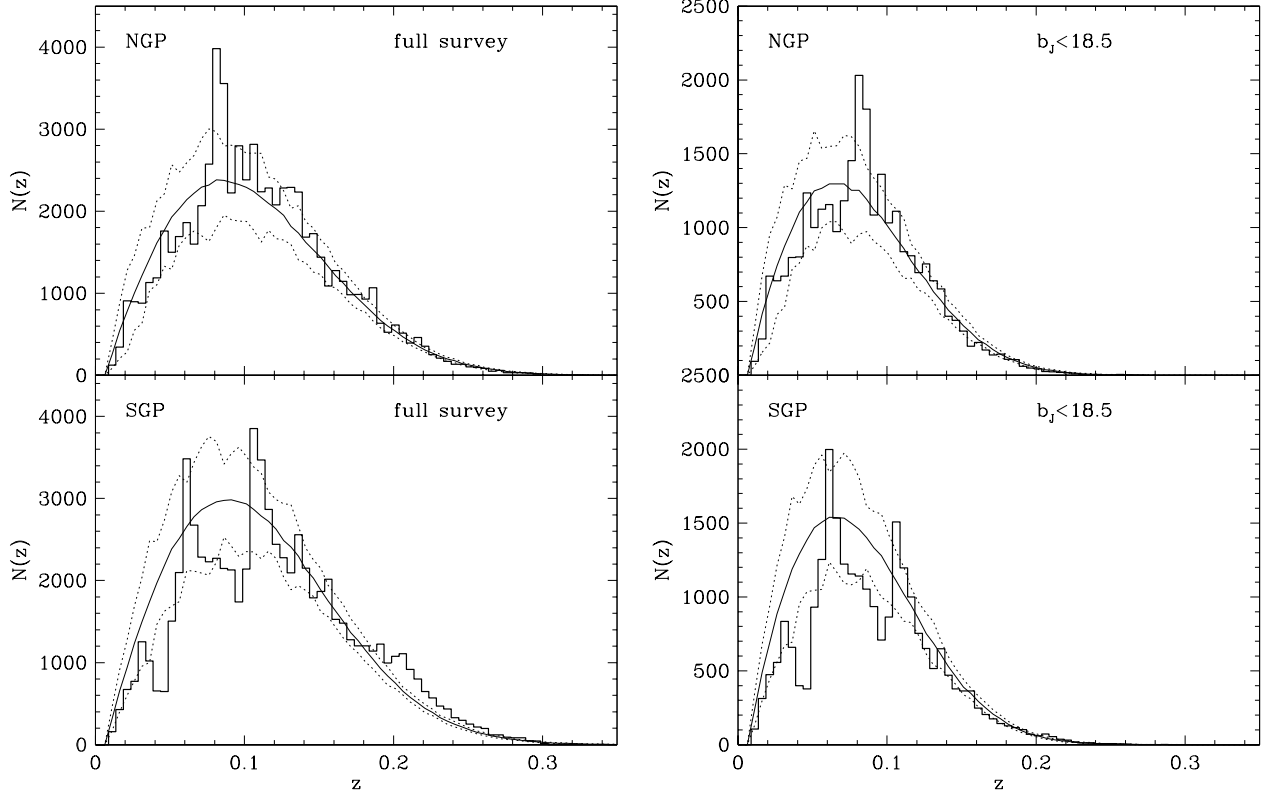


Figure 12. Redshift distributions in the 2dFGRS and mock catalogues. The histograms show the observed redshift distribution in the NGP and SGP regions of the 2dFGRS. The left-hand panels are to the full depth of the survey while the right-hand panels include only galaxies brighter than $b_J = 18.5$. The smooth solid curves show the predicted redshift distributions based on our Schechter function estimate of the galaxy luminosity function, including the magnitude measurement errors, the variation in the survey magnitude limit and the dependence of completeness on apparent magnitude. The dotted lines indicate the rms variation in the redshift histograms within our ensemble of 22 mock galaxy catalogues.

galaxies which make it into the 2dFGRS are one to two magnitudes brighter than M^* , where the galaxy luminosity function is very steep. Thus, a small shift in magnitude can result in a large change in the number of galaxies brighter than the survey magnitude limit. Brightening M^* in the SGP by just 0.06 magnitudes would boost the predicted high- z $N(z)$ and produce a model that better matches the observed distribution. Another possibility that needs further investigation is that the random magnitude measurement errors become larger for faint objects at high z . A trend of this sort is not evident in the comparison we have made between 2dFGRS and SDSS EDR magnitudes in Fig 2, but this comparison pertains to the NGP only. For now one should be careful, as we have been in previous papers, to ensure that large-scale clustering results are not strongly influenced by this feature. For instance, the estimate of the large scale galaxy power spectrum in Percival et al. (2001) used separate selection functions, which empirically matched the high- z $N(z)$ in both NGP and SGP.

10 DISCUSSION AND CONCLUSIONS

We have used the CCD data of the SDSS EDR (Stoughton et al. 2001) to assess the accuracy and completeness of the 2dFGRS photometric catalogue, which is based on APM scans

of the UKST photographic plates (Maddox et al. 1990b). We find that the measurement errors in the APM magnitudes are in agreement with previous estimates, having a $1-\sigma$ spread (robustly estimated) of 0.164 magnitudes. We find a small zeropoint offset between the SDSS EDR and the 2dFGRS photometry of $|\Delta| = 0.058$ and no evidence for any scale error in the magnitude calibration in the range $17 < b_J < 19.5$. As more calibrating data become available, the accuracy of both the 2dFGRS and SDSS photometric zeropoints should be improved. We find that compared to the SDSS photometric catalogue, the 2dFGRS parent catalogue is $87 \pm 2\%$ complete. This is close to the original estimates based on the accuracy of star-galaxy classification in the APM catalogue (Maddox et al. 1990a). The reasons behind the $13 \pm 2\%$ of galaxies that are missed are investigated in more detail in Cross et al. (2001b), who compare the 2dFGRS parent catalogue with the MGC, a deep, wide area B-band CCD imaging survey (Lemon et al. 2001). They find that mis-classification (e.g. galaxies incorrectly classified as merged images or stars) is the largest cause of incompleteness, but also a small population of low surface brightness galaxies is missed.

Making simple statistical corrections for incompleteness, magnitude measurement errors and uncertainties in modelling evolution and k-corrections, we find that the true $z = 0$ galaxy luminosity function is accurately described

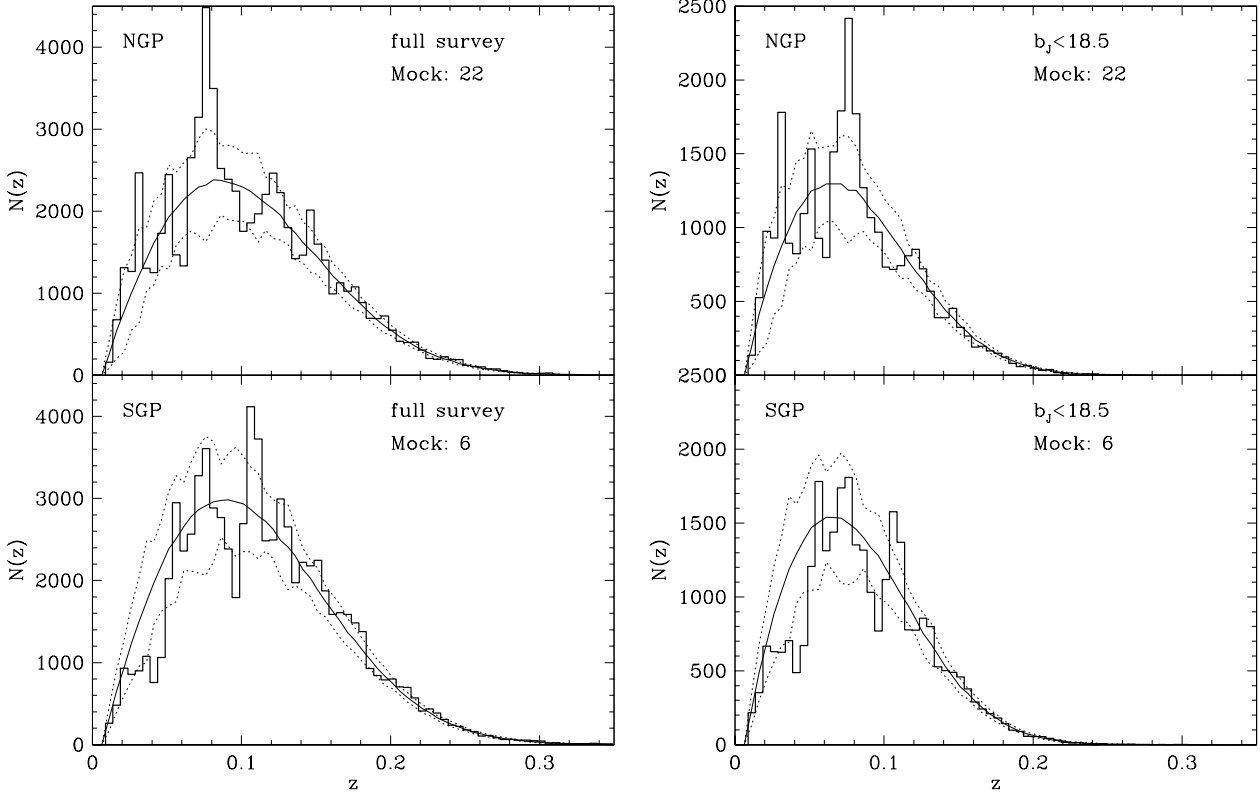


Figure 13. As Fig. 12, but for two selected mock catalogues rather than the genuine 2dFGRS.

by a Schechter function with parameters: $M_{b_J}^* - 5\log_{10} h = -19.66 \pm 0.07$, $\alpha = -1.21 \pm 0.03$ and $\Phi^* = (1.68 \pm 0.08) \times 10^{-2} h^3 \text{Mpc}^{-3}$ (assuming an $\Omega_0 = 0.3$, $\Lambda_0 = 0.7$ cosmology). With over 110 500 redshifts, the statistical errors in our estimate are negligible compared to the systematic errors (i.e. uncertainties that cause an overall shift of the luminosity function) from fluctuations produced by large-scale structure and by the uncertainty in the evolutionary corrections. Our quoted errors include estimates of these uncertainties, the former derived from extensive, realistic mock catalogues.

Taking account of the photometric zeropoint difference, random magnitude measurement errors, and using an accurate colour equation, we find very good agreement between the form of the b_J -band LF inferred from the SDSS data and the 2dFGRS estimate. Also, in the area of overlap, the 2dFGRS and SDSS galaxy counts agree at $b_J = 19.2$. This is the magnitude at which we use the counts to normalize our luminosity function. Thus, when normalized in the same way, 2dFGRS and SDSS b_J -band LF estimates agree with great accuracy. Blanton et al. (2001) reached a different conclusion principally because they used an inaccurate colour equation to convert from SDSS wavebands to b_J and did not take account of galaxy evolution.

The integrated $z = 0$ b_J -band luminosity density implied by the 2dFGRS LF is $(1.90 \pm 0.18) \times 10^8 h \text{L}_\odot \text{Mpc}^{-3}$. This is in good agreement with earlier estimates from the 2dFGRS presented in Folkes et al. (1999) and Madgwick et al. (2001) although neither of these estimates took account of the small effect of modelling evolution and the Folkes et al. estimate assumed an $\Omega_0 = 1$ cosmology. Also it agrees well

with the estimate made by Cross et al. (2001a) which took account of the dependence of galaxy selection on surface brightness. Their result, which is normalized to the MGC region whose density is 5% greater than the mean in the 2dFGRS, is $\rho_L = 2.16 \times 10^8 h$ (when converted to solar units using $M_{b_J}^* = 5.3$). This close agreement indicates that surface brightness issues do not represent a major uncertainty in these estimates of the luminosity density.

It has been highlighted by Wright (2001) that the luminosity density measured in the optical bands by the SDSS (Blanton et al. 2001), combined with a simple model for the expected spectrum, predicts a luminosity density in the K_S -band a factor of 2.3 greater than the value measured in the joint analysis of 2MASS (Jarrett et al. 2000) and 2dFGRS presented in Cole et al. (2001). Even if the SDSS luminosity densities were to be revised downwards to agree with the 2dFGRS in the b_J -band, the discrepancy in the K_S -band would only be reduced to a factor of 1.6. Furthermore, the correction for longer wavelength bands is likely to be smaller than that we have inferred for the g -band. Thus, a puzzling factor of approximately 1.8 to 2 remains between the K_S -band luminosity density measured from 2MASS and that inferred by extrapolation from the optical bands.

Wright (2001) speculated that the 2MASS magnitudes could be grossly underestimated. This possibility is ruled out by the comparison of 2MASS magnitudes with Kron magnitudes measured from deeper images of the same objects by Loveday (2000), presented by Cole et al. (2001). Also, combining the 2MASS and SDSS EDR magnitudes for matched objects, we find optical to near infrared colours which, on

average, agree well with the mean galaxy spectrum adopted by Wright. A second speculation made by Wright was that perhaps the 2MASS extended source catalogue is incomplete and misses a significant fraction of the galaxies that SDSS detects. This is also ruled out. The assessment of the completeness of 2dFGRS compared to 2MASS presented in Cole et al. (2001), together with the assessment of the 2dFGRS completeness with respect to the SDSS presented here, shows that the 2MASS and SDSS source densities agree to about 2%.

The most likely cause of the discrepancy between the K_S-band and extrapolated optical luminosity densities is large-scale structure. Since the 2MASS survey has a much brighter limiting magnitude than either the 2dFGRS or SDSS, their luminosity functions are not normalized within the same volume. Cole et al. (2001) normalized their K_S-band LF using an estimate of the counts from a small, 184 deg² area (Jarrett et al. in preparation) and an indirect estimate from the approximately 619 deg² of overlap between 2MASS and 2dFGRS. The second estimate is not direct, and is perhaps not highly accurate, because it requires an estimate of the effective area of sky in the intersection of the 2dFGRS and 2MASS. This is not trivial to obtain because a map of the 2MASS sky coverage is not yet available. Cole et al. (2001) estimated that large-scale structure would cause a 15% variation in the number counts within a 619 deg² area. Our mock catalogues, modified to mimic the selection criteria of the 2MASS, show that the rms variation in the counts over a 184 deg² area is, significantly larger, 19%. Thus, it will be very interesting to derive the K_S-band counts over a larger area, which should soon become possible with a more complete 2MASS catalogue, to see whether the estimates of the J and K_S-band luminosity densities and the inferred stellar density need to be revised.

We have described maps that define the redshift completeness of the current 2dFGRS catalogue and the weak dependence of the degree of completeness on apparent magnitude. These, together with the luminosity function and a map of the survey magnitude limit, provide a complete description of the 2dFGRS selection function. We have created mock galaxy catalogues from cosmological N-body simulations using this description of the selection function. Comparison of these with the observed data indicates that, in general, the data are well described by our selection function and exhibit fluctuations that are typical of those expected in the standard Λ CDM cosmology.

ACKNOWLEDGEMENTS

The data used here were obtained with the 2 degree field facility on the 3.9m Anglo-Australian Telescope (AAT). We thank all those involved in the smooth running and continued success of the 2dF and the AAT.

REFERENCES

Arnouts S., de Lapparent V., Mathez G., Mazure A., Mellier Y., Bertin E., Kruszewski A., 1997, A&AS, 124, 163

Arnouts S., et al. , 2001, A&A, submitted. (astro-ph/0103071)

Baugh C. M., Efstathiou G., 1993, MNRAS, 265, 145

Baugh C.M., Branchini E., Cole S., 2001 in preparation

Blair M., Gilmore G., 1982, PASP, 94, 741

Blanton M.R., et al. 2001, AJ, 121, 2358 (astro-ph/0012085)

Bruzual A. G., Charlot S., 1993, ApJ, 405, 538

Charlot S., Longhetti M., 2001, MNRAS, 323 887

Cole S., Aragon-Salamanca A., Frenk C.S., Navarro J.F., Zepf S.E., 1994, MNRAS, 271, 781

Cole S., Hatton S., Weinberg D.H., Frenk C.S., 1998, MNRAS, 300, 945

Cole S., Lacey C.G., Baugh C.M., Frenk C.S., 2000, MNRAS, 319, 168

Cole S., et al. (The 2dFGRS Team) 2001, MNRAS, 326, 255

Colless M., et al. (the 2dFGRS team) 2001, MNRAS, in press (astro-ph/0106498)

Cross N.J.G., et al. (The 2dFGRS Team) 2001a, MNRAS, 324, 825

Cross N.J.G., & Driver, S.P. 2001, MNRAS, in press. (astro-ph/0110402)

Cross N.J.G., et al. (The 2dFGRS Team) 2001b, in preparation.

Davis M., Huchra J., 1982, ApJ, 254, 437

Driver S.P., 1999, ApJ, 526, L69

Efstathiou G., Ellis R.S., Peterson B.A., 1988, MNRAS 232, 431

Evrard A.E., 1999, in proceedings of the MPA-ESO cosmology conference 1998, "Evolution of large scale structure : from recombination to Garching" eds A. J. Banday, R. K. Sheth, and L. N. da Costa, Garching, Germany : European Southern Observatory, p.249 (astro-ph/9812377)

Evrard A.E., et al. 2001, ApJ submitted (astro-ph/0110246)

Felten J. E., 1976, ApJ 207, 700

Ferguson H.C., Binggeli B., 1994, A&AR 6, 67

Folkes S., et al. (2dFGRS Team), 1999, MNRAS, 308, 459

Fukugita M., Ichikawa T., Gunn J.E., Doi M., Shimasaku K., Schneider D.P., 1996, AJ, 111, 1754

Jarrett T.H., Chester T., Cutri R., Schneider S., Skrutskie M., Huchra, J.P., 2000, AJ, 119, 2498

Kauffmann G., White S.D.M., Guiderdoni B., 1993, MNRAS, 264, 201

Lemon D.J., Liske J., Driver S.P., Cross N.J.G., Couch W.J., 2001, in preparation

Liu M.C., Charlot S., Graham J.R., 2000, ApJ, 543, 644

Loveday J., Peterson B. A., Efstathiou G., Maddox S.J., 1992, ApJ, 390, 338

Loveday J., 2000, MNRAS, 312, 517

Maddox S.J., Sutherland W.J., Efstathiou G., Loveday J., Peterson B.A., 1990, MNRAS, 247, 1

Maddox S.J., Efstathiou G., Sutherland W.J., Loveday J., 1990a, MNRAS 243, 692

Maddox S.J., Efstathiou G., Sutherland W.J., Loveday J., 1990b, MNRAS 246, 433

Maddox S.J., Efstathiou G., Sutherland W.J., Loveday J., 1996, MNRAS 283, 1227

Maddox S.J., et al., (The 2dFGRS Team) 2001, in preparation.

Madgwick D.S., et al. , (The 2dFGRS Team), 2001, MNRAS submitted. (astro-ph/0106498)

Marzke R.O., Huchra J.P., Geller M.J., 1994, ApJ., 428, 43

Metcalfe N., Fong R., Shanks T., 1995, MNRAS, 274, 769

Norberg, P., et al. (The 2dFGRS Team) 2001a, MNRAS, in press.

Norberg, P., et al. (The 2dFGRS Team) 2001b, MNRAS, in preparation.

Norberg, P., 2001c, Durham University Ph.D. Thesis.

Pimbblet K.A., Smail I., Edge A.C., Couch W.J., O'Hely E., Zabludoff A.I., 2001, MNRAS, 327, 588

Percival W.J., et al. (The 2dFGRS Team) 2001, MNRAS, 327, 1297 (astro-ph/0105252)

Prandoni I., et al. 1999, A&A 345, 448

Sandage A., Tammann G.A., Yahil A., 1979, ApJ 232, 352

Schechter P., 1976, ApJ, 203, 297

Somerville R., Primack J.R., 1999, MNRAS, 310, 1087

Stoughton C., et al. , (The SDSS Collaboration), 2001 in preparation
 White S.D.M., Frenk C.S., 1991, ApJ, 379, 52
 Wright E.L., 2001, ApJ, 556, 17
 Yasuda N., et al. 2001, (The SDSS Collaboration) AJ, 122, 1104 (astro-ph/0105545)
 Zucca E., et al. 1997, A&A, 326, 477

APPENDIX A: REDSHIFT INCOMPLETENESS IN THE 2dFGRS

When complete, the fraction of redshifts measured should be uniformly high across the full area of the 2dFGRS. However, at this intermediate stage, when only a subset of the target 2dF fields have been observed, the fraction of redshifts measured varies considerably with position. As detailed in Section 8 of Colless et al. (2001), this variation is best quantified by dividing the survey into sectors (labelled by an angular position $\boldsymbol{\theta}$) defined by the overlaps of the target 2dF fields. Within each of these sectors one can calculate the fraction $R(\boldsymbol{\theta})$ of the parent catalogue galaxies whose redshifts have been measured. It is this completeness map, pixelated for convenience, that is shown in Fig. 1.

In contrast to most previous redshift surveys, the 2dFGRS is so large that residual small systematic errors can begin to dominate over statistical errors. For this reason, we have developed a quantitative description of the dependence of the completeness on apparent magnitude. Note that 76% of the observed fields have an overall completeness of greater than 90% (this should increase with time as some of the lower completeness fields are re-observed) and so generally incompleteness and its dependence on apparent magnitude are small. In Section 8.3 of Colless et al. (2001), we showed that for each observed field the dependence of the redshift completeness on apparent magnitude could be described by a one parameter function (see figure 16 of Colless et al. 2001)

$$c_z(b_J, \mu_i) = 0.99 (1 - \exp[b_J - \mu_i]). \quad (A1)$$

Here b_J is the apparent magnitude and μ_i is the value of the parameter for field i . In each sector, the targeted galaxies are split between several fields and so one must define an appropriately averaged value, $\mu(\boldsymbol{\theta})$, for each sector. This can be derived by writing the magnitude-dependent redshift incompleteness of a sector $c_z(b_J, \mu(\boldsymbol{\theta}))$ as a weighted sum of the completeness of its $N_F(\boldsymbol{\theta})$ component fields,

$$c_z(b_J, \mu[\boldsymbol{\theta}]) = \sum_{i=1}^{N_F(\boldsymbol{\theta})} f_i c_z(b_J, \mu_i), \quad (A2)$$

where f_i is the fraction of observed galaxies in this sector that were targeted in field i . Hence by identification of terms

$$c_z(b_J, \mu_i) = 0.99 (1 - \exp[b_J - \mu(\boldsymbol{\theta})]), \quad (A3)$$

where

$$\mu(\boldsymbol{\theta}) = -\ln \left[\sum_{i=1}^{N_F(\boldsymbol{\theta})} f_i \exp(-\mu_i) \right]. \quad (A4)$$

With this one can define the function

$$S(\boldsymbol{\theta}, b_J) = \frac{N_p(\boldsymbol{\theta})}{N_e(\boldsymbol{\theta})} R(\boldsymbol{\theta}) c_z(b_J, \mu[\boldsymbol{\theta}]), \quad (A5)$$

which is an estimate of the fraction of galaxies of apparent magnitude b_J in the sector at position $\boldsymbol{\theta}$ that have redshift measurements. Here $N_p(\boldsymbol{\theta})$ is the number of galaxies in the parent 2dFGRS catalogue that fall in the sector and

$$N_e(\boldsymbol{\theta}) = \sum_{j=1}^{N_p(\boldsymbol{\theta})} c_z(b_J^j, \mu[\boldsymbol{\theta}]) \quad (A6)$$

is an estimate of the number of these galaxies for which one would expect to have measured redshifts given the value of $\mu(\boldsymbol{\theta})$.

Maps of $b_J^{\lim}(\boldsymbol{\theta})$, $R(\boldsymbol{\theta})$ and $\mu(\boldsymbol{\theta})$ together with associated software are available for the 2dFGRS data in the “100k Release” (<http://www.mso.anu.edu.au/2dFGRS/>). Here, we employ the method described in section 8 of in Colless et al. (2001) to generate these quantities for the more extensive dataset used in this paper. The map of $R(\boldsymbol{\theta})$ is shown in Fig. 1 and the corresponding map of $\mu(\boldsymbol{\theta})$ is shown in Fig. A1.

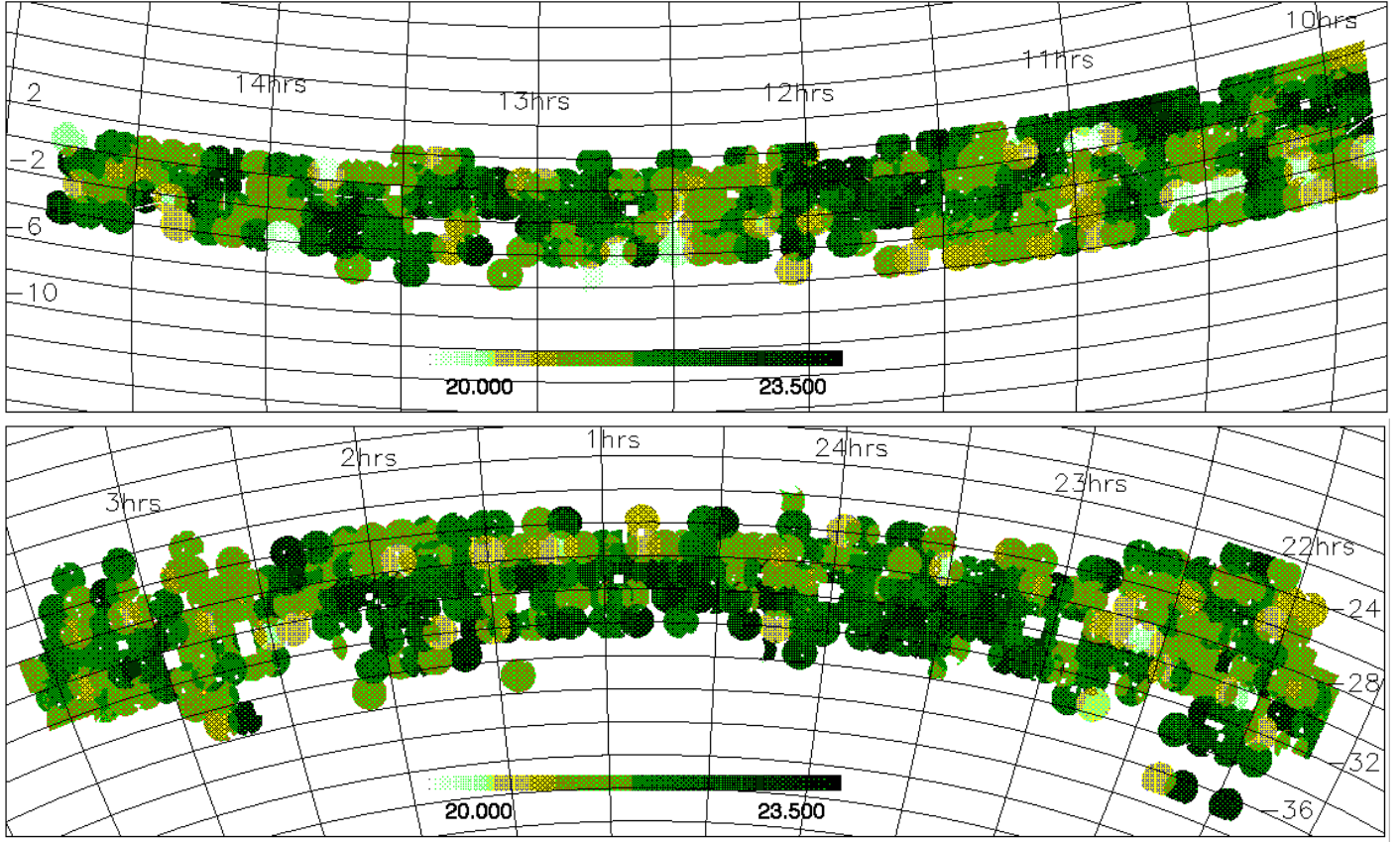


Figure A1. Map showing the variation of the parameter μ with position on the sky. The dependence of the redshift completeness on apparent magnitude is accurately described by the fitting function $c_z(b_J, \mu) = 0.99 (1 - \exp[b_J - \mu])$.